frontiers in Chemical Biology

TYPE Original Research
PUBLISHED 09 July 2026
DOI 10.3389/fchbi.2026.1848258

OPEN ACCESS

EDITED BY
Leticia Pérez Díaz,
University of the Republic, Uruguay

REVIEWED BY
Alicia Ponte-Sucre,
Central University of Venezuela, Venezuela
Mulate Zerihun,
Bar-Ilan University, Israel

*CORRESPONDENCE
Guillermo R. Labadie,
labadie@iquir-conicet.gov.ar

RECEIVED 06 April 2026
REVISED 16 May 2026
ACCEPTED 29 May 2026
PUBLISHED 09 July 2026

CITATION
Ballari MS, Damasceno FS, Merli ML, Fargnoli L, Pagura L, Cricco JA, Silber AM and Labadie GR (2026) Unravelling the effects of proline analogues against *Trypanosoma cruzi*. *Front. Chem. Biol.* 5:1848258. doi: 10.3389/fchbi.2026.1848258

Unravelling the effects of proline analogues against *Trypanosoma cruzi*

María Sol Ballari[1], Flávia S. Damasceno[2], Marcelo L. Merli[3], Lucía Fargnoli[1], Lucas Pagura[3], Julia A. Cricco[3], Ariel M. Silber[2] and Guillermo R. Labadie[1,4]*

[1]Instituto de Química de Rosario (IQUIR), Facultad de Ciencias Bioquímicas y Farmacéuticas, Universidad Nacional de Rosario, Rosario, Argentina, [2]Laboratory of Biochemistry of Tryps -LaBTryps, Departamento de Parasitologia, Instituto de Ciências Biomédicas, Universidade de São Paulo, Cidade Universitária, São Paulo, Brazil, [3]Instituto de Biología Molecular y Celular de Rosario (IBR), Consejo Nacional de Investigaciones Científicas y Técnicas CONICET – Facultad de Ciencias Bioquímicas y Farmacéuticas, Universidad Nacional de Rosario, Rosario, Argentina, [4]Departamento de Química Orgánica, Facultad de Ciencias Bioquímicas y Farmacéuticas, Universidad Nacional de Rosario, Rosario, Argentina

Background: Proline is a fundamental amino acid for *T. cruzi*, the etiological agent of Chagas disease. Proline is mainly incorporated from the extracellular medium by amino acid transport systems. Different proline analogues proved to interact with the proline permease TcAAAP069 and inhibit proline uptake by *T. cruzi*.
Methods: Decyl- (**1**), oleyl- (**2**) and farnesyl- (**3**) substituted proline analogues were evaluated on 6 *T. cruzi* DTUs. Effects on cell death and cell cycle were determined by flow cytometry. A fluorescent tag was incorporated to compound **1** (**1-NBD**), in order to follow-up its fate through fluorescence microscopy and to determine its localization. The structure–activity relationship (SAR) was extended in order to understand the role of the proline and triazole motifs (compounds **4** – **13**).
Results: The compounds showed broad-spectrum activity against all DTUs. Compound **2** induced an apoptosis-like cell death phenotype, while compounds **1** and **3** induced cell cycle arrest at G1. The fluorescent labelling (**1-NBD**) and subsequent microscopy showed that compound **1** can be taken up by epimastigotes. SAR showed that triazole is crucial for activity, while proline grants selectivity, being the proline-triazole hybrid being essential for their activity, and the nature of the alkyl chains significantly influences their mode of action.
Conclusion: These findings contribute to a deeper understanding of the role of proline uptake and metabolism in *T. cruzi* survival.

KEYWORDS
cell cycle arrest, cell death, fluorescence microscopy, NBD, proline transport, structure, activity relationship, Trypanosoma cruzi

1 Introduction

Chagas disease, whose etiological agent is *T. cruzi*, is a parasitic disease classified within the group of neglected tropical diseases (NTDs). It constitutes a significant public health problem in the Americas. The genetic, biochemical and biological diversity of *T. cruzi* strains has long been recognized through both ecological and epidemiological complexity (Campbell et al., 2004; Miles et al., 2009; Zingales et al., 2009).

Throughout its life cycle, *T. cruzi* can withstand different extracellular conditions in the insect intestine, mammalian bloodstream and the different host-cells cytoplasm. Each of these environments provide the parasite with distinct metabolites for survival, proliferation

and infection. Consequently, the parasite acquired evolutionary adaptations, including its ability to rapidly switch from a carbohydrate-based metabolism (Barros-Álvarez et al., 2014; Barisón et al., 2017) to fatty acids- (Oliveira Souza et al., 2021) or amino acids-based metabolism. Among these adaptations, the relevance of proline metabolism was early recognized (Sylvester and Krassner, 1976).

Among the amino acids, proline has demonstrated its multifunctional role in *T. cruzi*. It is known that this amino acid, or the intermediates of its metabolism, induce metacyclogenesis, a process in which the epimastigote forms differentiate into metacyclic trypomastigotes, in the final portion of the intestine of the insect vector (Contreras et al., 1985). The role of proline as an oxidizable metabolite during proliferation in host cells (Silber et al., 2009) and in the differentiation of intracellular epimastigote forms to trypomastigotes (Tonelli et al., 2004) was also demonstrated. More recently, it was shown that proline is the energetic support in cell invasion in the vertebrate host (Martins et al., 2009). In that work, it was demonstrated that, under conditions of nutritional depletion, the parasite considerably reduces intracellular ATP levels as well as its ability to infect mammalian cells, a condition that is reversed after the addition of proline to the medium. Proline is also involved in resistance to different types of stress, in particular oxidative stress (Magdaleno et al., 2009; Paes et al., 2013). A study showed that parasites overexpressing a transporter for proline have a higher intracellular concentration of this amino acid, as well as an increased resistance to reactive oxygen species, such as hydrogen peroxide and nitric oxide, as well as trypanocidal drugs (Saye et al., 2014). It was also proposed proline's participation in a redox shuttle able to rebalance the redox power between the cytosol and the cell single mitochondrion (Marchese et al., 2020).

It is known that proline is oxidized to glutamate in two enzymatic steps: first, Proline Dehydrogenase (TcPRODH) oxidizes proline to Δ1-pyrroline-5-carboxylate (P5C), which is subsequently converted into glutamate by P5C Dehydrogenase (TcP5CDH) in presence of $NAD(P)^+$. It has been described that proline oxidation occurs in the mitochondria, stimulating cellular respiration and leading to the synthesis of ATP through the process of oxidative phosphorylation (Paes et al., 2013; Mantilla et al., 2015). Then, glutamate can be incorporated into the Krebs Cycle within the mitochondria (Silber et al., 2005), by transferring its amino group to pyruvate by Tyrosine Aminotransferase (TAT) (which also has Alanine Aminotransferase activity - ALAT), producing alanine and α-ketoglutarate (α-KG) (Zelada et al., 1996; Nowicki and Cazzulo, 2008).

Proline can be taken up from the extracellular medium by two active transporters (Silber et al., 2002; Saye et al., 2014), or it can be biosynthesized from glutamate in two enzymatic steps (Mantilla et al., 2017; Marchese et al., 2020). Two proline transport systems with varying affinities have been biochemically characterized in *T. cruzi*, and one proline transporter has been identified, the TcAAAP069 (Silber et al., 2002; Saye et al., 2014). This carrier belongs to the first multigenic family of amino acid transporters discovered in *T. cruzi*, the *T. cruzi* Amino Acid/Auxin Permeases (TcAAAP) (Bouvier et al., 2004). This transporter family is absent in mammals, and its members play a crucial role in *T. cruzi*'s ability to incorporate essential metabolites from the extracellular media, such as amino acids and polyamines. As a result, the TcAAAP family presents a promising potential as drug targets, but it also constitutes a potential new way to incorporate drugs into the parasite.

Currently, the arsenal of medications available for the treatment of Chagas disease is limited to Nifurtimox and Benznidazole. These drugs were developed over 50 years ago (Bermudez et al., 2016), and they are used despite the side effects and toxicity described, due to the lack of a better option. Despite these drugs being effective in the acute phase of the disease, their efficiency decreases in the chronic phase, when the toxicity and other adverse effects become more frequent. The complexity of the life cycle of *T. cruzi* (Duschak, 2019), which consists of various stages of the parasite and biochemical changes associated with interactions between the parasite and its host, hinder the development of new drugs (De Souza, 2002). In this context, there is a growing need to validate new therapeutic targets for the development of effective drugs for the treatment of the disease.

In this context, chemical probes are indispensable tools for functionally dissecting putative targets like TcAAAP069. Small molecule inhibitors can provide acute, tuneable, and reversible interference, offering insights into the immediate physiological consequences of target modulation that complement genetic approaches. Previously, we designed and synthesized a library of L-proline analogues and identified four analogues with IC_{50} values under 50 μM in CL14 strain *T. cruzi* epimastigotes (Fargnoli et al., 2020). These values were significantly lower than L-thiazolidine-4-carboxylic acid (T4C, IC_{50} = 890 μM), the only proline uptake inhibitor with reported activity on *T. cruzi* (Magdaleno et al., 2009). Mechanistically, we demonstrated that two of those analogues (**1** and **3**, Figure 1) function as inhibitors of proline uptake via the TcAAAP069 transporter (Sayé et al., 2017). Notably, these assays highlighted that both compounds exhibited different types of transport inhibition.

Building on this foundation, the present work employs these proline analogues as chemical probes to systematically investigate the biological role and druggability of the proline transport system in *T. cruzi*. We evaluate their activity across 6 *T. cruzi* DTUs, establishing their broad-spectrum potential—a critical step given the clinical relevance of strain diversity in Chagas disease. We delineate the distinct phenotypic outcomes (cytostasis vs. cytotoxicity) arising from transport inhibition versus off-target effects. Using a fluorescent conjugate, we visualize probe internalization. Finally, through a focused structure-activity relationship study, we define the molecular features essential for potency and selectivity. Collectively, this chemical biology approach aims to further evaluate proline transport as a candidate therapeutic target and provide a mechanistic framework for future inhibitor design.

2 Results

2.1 Unveiling the antiparasitic potential of proline analogues across *T. cruzi* DTUs

The complex *T.* cruzi intra-species diversity led to define a sub-species taxon including six groups named discrete typing units (DTUs: TcI–VI) (Zingales et al., 2009; Zingales, 2018). These DTUs exhibit differences in infectivity for various vector species,

10.3389/fchbi.2026.1848258

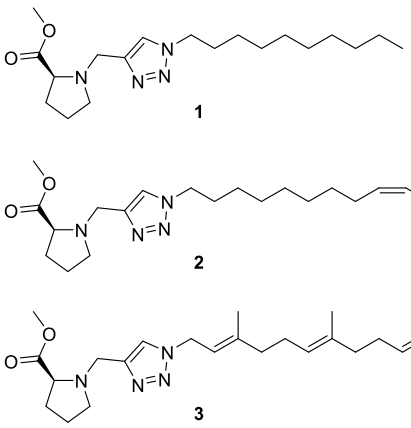

FIGURE 1
L-proline analogues under study (Sayé et al., 2017; Fargnoli et al., 2020). **1**: Methyl ((1-decyl-1H-1,2,3-triazol-4-yl)methyl)-L-prolinate; **2**: Methyl (Z)-((1-(octadec-9-en-1-yl)-1H-1,2,3-triazol-4-yl)methyl)-L-prolinate; **3**: Methyl ((1-((2E,6E)-3,7,11-trimethyldodeca-2,6,10-trien-1-yl)-1H-1,2,3-triazol-4-yl)methyl)-L-prolinate.

host cells, virulence, capacity to induce injury, tropism, antigenic constitution, growth rates, and susceptibility to chemotherapeutic agents (Lages-Silva et al., 2001; Zingales et al., 2012). According to DND*i*, an acceptable Target Product Profile should involve at least the inhibition of the proliferation of *T. cruzi* DTUs I, II, V and VI, but ideally a drug should inhibit the proliferation of all DTUs (Kratz, 2019). Taking this into account, we embarked on a study to determine the antiparasitic activity of our compounds against representative strains of each one of the six DTUs. Therefore, compounds **1** - **3** were tested against epimastigotes from strains belonging to DTUs TcI to TcVI. The effects these compounds exerted on each DTU (initial epimastigote concentration: 2.5 × 10^6 cells/mL) were monitored for 6–11 days, and IC_{50} values were determined when the parasites were in the mid-exponential growth phase. Proliferation and dose-response curves were obtained for the three analogues for each representative of the six DTUs. (See, Supplementary Figures S1–S6). Importantly, the analogues were active against all DTUs with IC_{50} values ranging between 20 and 57 μM (Table 1). Specifically, among the three compounds under study, the strain belonging to TcV (92:80) exhibited higher susceptibility. The strain belonging to TcIV was the most resistant to compound **1**, and the strain belonging to TcVI was less susceptible to compound **3**, compared to the other strains. These results illustrate that the proline analogues have a broad-spectrum effect against the different *T. cruzi* DTUs.

2.2 Unravelling the trypanocidal and trypanostatic properties of proline analogues on *T. cruzi*

To comprehensively investigate the trypanocide or trypanostatic nature of compounds **1**, **2** and **3**, an analysis encompassing cell death, cell cycle and washout effects were conducted. The CL14 strain (TcVI) was selected for these mechanistic studies on the basis of physiological and practical considerations: among the six DTU-representative strains evaluated here, CL14 displayed the shortest doubling time (~17 h, Table 1), allowing flow-cytometry endpoints (cell death, cell cycle, washout) to be sampled at well-defined points of exponential proliferation within standard 24–72 h windows; in addition, CL14 is well characterized in our hands and was the strain used to define the original IC_{50}-IC_{80} range for these compounds (Fargnoli et al., 2020), enabling direct comparison with our previous data. We acknowledge, however, that mode-of-action conclusions drawn from a single fast-growing TcVI strain should be extended to other DTUs in future work. Accordingly, *T. cruzi* CL14 epimastigotes were subjected to treatments with compounds **1**, **2** or **3** at concentrations corresponding to their IC_{50} or IC_{80} values. Specifically, compound **1** exhibited an IC_{50} of 39 μM and an IC_{80} of 74 μM, while compound **2** showed an IC_{50} of 35 μM and an IC_{80} of 54 μM. Compound **3** has an IC_{50} of 49 μM and an IC_{80} of 116 μM. Simultaneously, untreated assays were performed as a negative control for each experiment.

To prove the compounds' influence on cell death mechanisms, we examined the presence of exposed phosphatidylserine, a canonical marker for programmed cell death (PCD) on the parasite's external surface and the possible membrane damage (an indicator of necrotic death) using a dual labelling with FITC-labelled Annexin-V (ANX) and propidium iodide (PI), followed by cytometry analysis at 24, 48 and 72 h post-treatment. Our results revealed a pronounced increase in ANX-labelled cells in response to treatment with compound **2**, most notably at 24-h treatment, consistent with an apoptosis-like cell death phenotype (Figures

TABLE 1 Inhibitory concentration (IC_{50}) determined for the proline analogues 1, 2 and 3 against *T. cruzi* epimastigotes (TcI to TcVI).

Geographical origin	Strain	DTU	Doubling time (h)	IC_{50} (μM)			pIC_{50} (μM)[a]		
				1	2	3	1	2	3
Pará (Br)	Sylvio	TcI	29.4	32.9 ± 4.5	38.7 ± 3.9	28.1 ± 1.9	1.5 ± 0.1	1.6 ± 0.1	1.4 ± 0.03
Sao Paulo (Br)	Y	TcII	24.6	37.6 ± 5.8	25.7 ± 5.2	25.8 ± 4.3	1.6 ± 0.1	1.4 ± 0.1	1.4 ± 0.1
Pará (Br)	M6241	TcIII	47.8	47.7 ± 8.9	39.8 ± 9.2	29.5 ± 6.1	1.7 ± 0.1	1.6 ± 0.1	1.5 ± 0.1
Pará (Br)	Can III	TcIV	46.7	56.8 ± 11.3	47.3 ± 11.5	39.7 ± 11.9	1.7 ± 0.1	1.7 ± 0.1	1.6 ± 0.1
St. Cruz (Bol)	92:80	TcV	69.3	20.7 ± 6.9	25.8 ± 7.6	26.3 ± 10.1	1.3 ± 0.1	1.4 ± 0.1	1.4 ± 0.2
Rgs (Br)	CL14	TcVI	16.9	39.0 ± 1.4	35.1 ± 7.0	48.3 ± 1.3	1.6 ± 0.02	1.5 ± 0.1	1.7 ± 0.01

[a]pIC_{50} = log (IC_{50} (μM)).

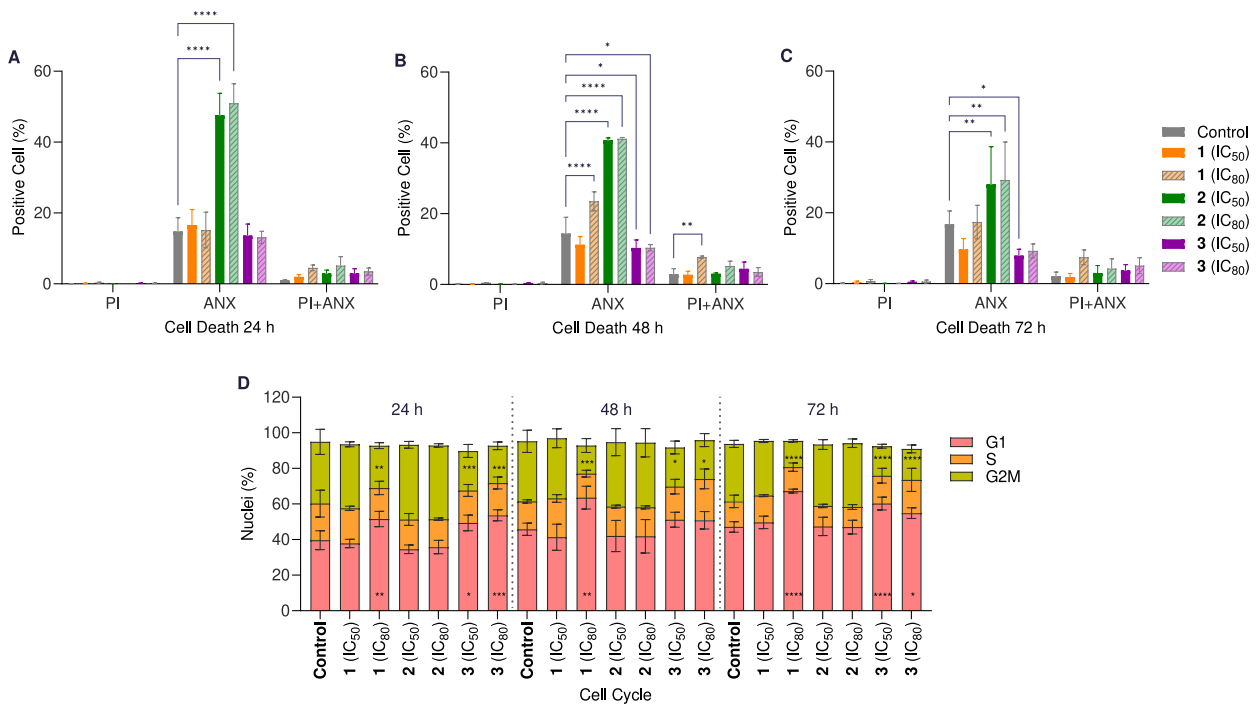

FIGURE 2
Cell death and cell cycle analysis for *T. cruzi* epimastigotes (CL14) treated with compounds **1**, **2** and **3** at their IC_{50} and IC_{80} concentrations. **1**: IC_{50} = 39 μM, IC_{80} = 74 μM; **2**: IC_{50} = 35 μM, IC_{80} = 54 μM; **3**: IC_{50} = 49 μM, IC_{80} = 116 μM. Data acquired by flow cytometry. **PI** = propidium iodide-labelled cells; **ANX** = FITC Annexin-V-labelled cells; **PI + ANX** = double-labelled cells. Cell death at 24 h **(A)**, 48 h **(B)**; or 72 h **(C)** post-treatment, Cell cycle at 24, 48 and 72 h **(D)** post treatment. Results are average of three independent measures. Significance levels calculated by two-way ANOVA at 95% confidence. *: $0.01 \leq p < 0.05$; **: $0.001 \leq p < 0.01$; ***: $0.0001 \leq p < 0.001$; ****: $p < 0.0001$.

2A–C, and Supplementary Figures S9–S10). For compound **1**, examination after a 48-h treatment highlighted a substantial increase in ANX and PI + ANX labelling at the IC_{80} concentration, suggesting early apoptosis and late apoptosis, characterized by loss of membrane integrity. This effect waned over time, likely attributed to compound consumption and diminishing concentration. In contrast, compound **3** displayed a minor reduction in ANX-labelled cells at 48 h, in the same level of the control, with no significant increments in PI or PI + ANX labelling. In sum, compounds **1** and **3** exhibited limited evidence of inducing apoptotic or necrotic cell death.

It is important to note the methodological limits of dual Annexin-V–FITC/propidium-iodide labelling for assigning a death modality in *T. cruzi*. Annexin-V detects surface phosphatidylserine (PS) and propidium iodide reports loss of plasma-membrane integrity; in classical mammalian models, Annexin-V^+/PI^- cells are taken as "early apoptotic", double-positive (Annexin-V^+/PI^+) cells as "late apoptotic/secondary necrotic", and Annexin-V^-/PI^+ cells as primary necrotic. In trypanosomatids, however, this assignment must be made with caution: PS exposure can occur without engagement of a canonical caspase-dependent apoptotic pathway, and double-positive populations cannot, on their own, distinguish bona fide programmed cell death from a regulated necrosis-like process. We therefore use the operational descriptor "apoptosis-like" throughout.Future studies combining orthogonal markers (e.g., loss of mitochondrial membrane potential, DNA fragmentation/TUNEL, cytochrome-*c* release, metacaspase or autophagy markers) will be required to formally classify the death pathway triggered by compound **2**.

Drawing on the outcomes of the cell death analysis, the study ventured into evaluating the potential of compounds **1** and **3** to induce cell cycle arrest in *T. cruzi*. This exploration revolved around specific cell cycle phases, encompassing G1, S, and G2M phases. For this, the cells treated for 24, 48 or 72 h (or untreated controls) were permeabilized with digitonine and labelled with propidium iodide, and further analyzed by cell cytometry. Compound **2** exhibited negligible influence on cell cycle progression, showing thus no impact on the parasite's cell cycle. In contrast, compound **1** at IC_{80} concentration, and compound **3** at both concentrations, engendered an accumulation of cells in the G1 phase, coupled with a reduction in the G2M cell population (Figure 2D and Supplementary Figures S14–S16). This effect displayed a gradual intensification over time, marked by an increment in G1 cells and a corresponding reduction in G2M cells. Collectively, these observations suggest that compounds **1** and **3** distinctly provoke a substantial disturbance in the cell cycle, resulting in G1 phase arrest and a decline in the G2M population.

To delve further into the reversible or irreversible effect of the drugs, the parasites were treated or not (control) with concentrations corresponding to the IC_{50} or IC_{80} of each compound for 48 h. After the treatment, the compounds were removed and the parasite's proliferation was recorded. A comparison of growth curves with and without parasite washout revealed that after washing out the

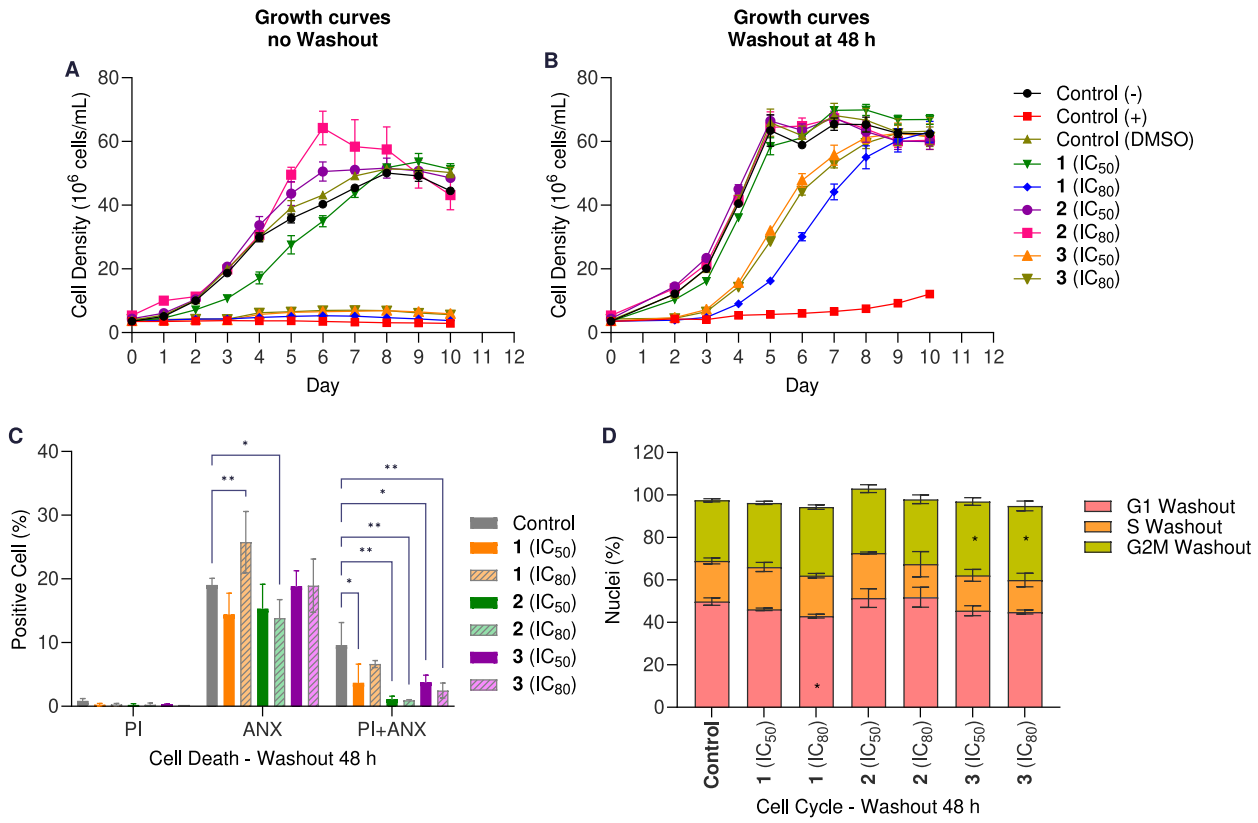

FIGURE 3
Washout experiments for T. cruzi epimastigotes (CL14) treated with compounds **1**, **2** and **3** at their IC_{50} and IC_{80} concentrations. **1**: IC_{50} = 39 μM, IC_{80} = 74 μM; **2**: IC_{50} = 35 μM, IC_{80} = 54 μM; **3**: IC_{50} = 49 μM, IC_{80} = 116 μM. **(A)** Growth curves with no washout performed; **(B)** Growth curves with washout performed at 48 h post-treatment; **(C)** Cell death analysis after washout at 48 h post-treatment; **(D)** Cell cycle analysis after washout at 48 h post-treatment. Results are representative of three independent measures. Significance levels calculated by two-way ANOVA at 95% confidence. *: $0.01 \leq p < 0.05$; **: $0.001 \leq p < 0.01$; ***: $0.0001 \leq p < 0.001$; ****: $p < 0.0001$.

drugs, the parasites treated with compounds **1** at a concentration equivalent to the IC_{50} or **2** at both concentrations proliferated at similar rates as the untreated control. However, those parasites treated with compound **1** at IC_{80} concentration and compound **3** at both concentrations showed a slower pace due to the diminished proliferating epimastigote concentration due to the treatment (Figures 3A,B and Supplementary Figure S8).

Furthermore, cell death and cell cycle analyses post-48 h treatment were pursued after the washout. In the cell death analysis, control cells demonstrated a surge in PI and PI + ANX labelling post-washout, suggesting potential cellular stress due to the washout procedure. However, no significant disparities were observed when comparing within compounds. For compound **1**, ANX labelling remained elevated compared to the control at IC_{80} concentration post-washout, with no discernible differences compared to its pre-washout state (48 h). Conversely, compound **2** exhibited post-washout cell growth and death patterns similar to the control, with ANX labelling reverting to similar levels. In the cell cycle analysis, cells previously treated with compounds **1** and **3** reverted to a normal cycle, indicating withdrawal of the cell cycle arrest (Figures 3C,D and Supplementary Figures S11–S13, S17). Notably, after washout, cultures previously exposed to compound **2** (which had induced an apoptosis-like phenotype) returned to proliferation rates and Annexin-V/PI profiles indistinguishable from untreated controls, whereas cultures previously exposed to compounds **1** and **3** (which had induced G1 arrest) recovered more slowly. Two interpretations should be considered: (i) the effects of these compounds are genuinely reversible upon removal, or (ii) the rebound reflects outgrowth of an unaffected sub-population from which damaged cells have been diluted out, rather than recovery of injured cells. Our present data do not formally distinguish between these possibilities; accordingly, throughout the manuscript, we use "trypanostatic" and "trypanocidal" in the operational sense of growth-inhibitory and cell-killing under the assay conditions employed, without claiming complete absence of lasting damage in the surviving population.

As a whole, the presented results indicate that, among the tested compounds, compound **2** induces an apoptosis-like cell death phenotype (operationally trypanocidal), while compounds **1** and **3** induce cell cycle arrest (trypanostatics). In all cases, treatment proved to be reversed upon removal.

2.3 Fluorescent analogue design and uptake assessment of L-Proline derivative in *T. cruzi* epimastigotes

To assess the potential uptake of L-proline analogue **1** by *T. cruzi* epimastigotes, we designed and synthesized a fluorescent variant

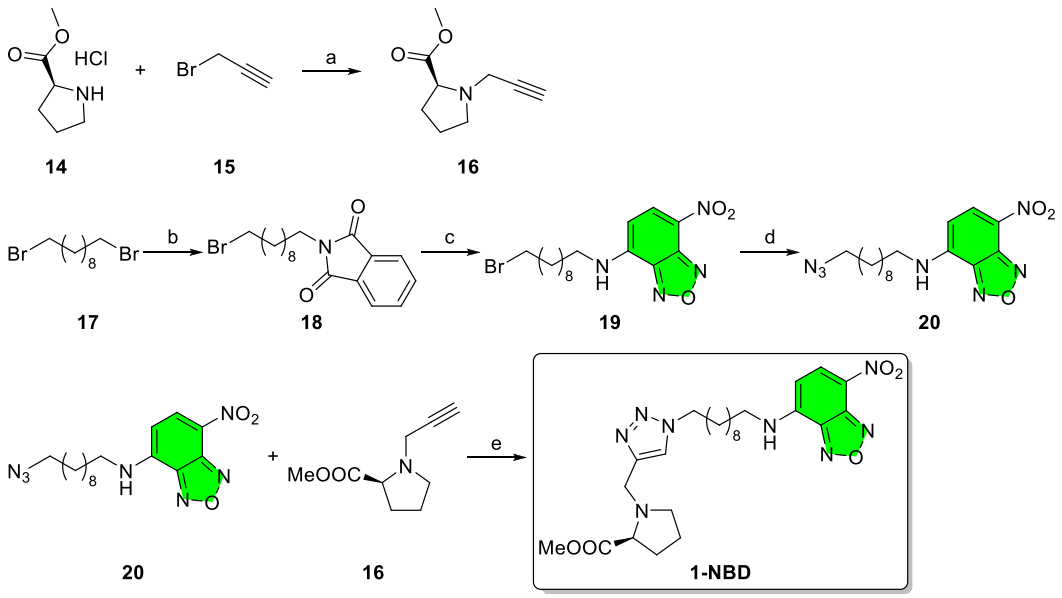

SCHEME 1
Synthesis of **1-NBD**. **(a)** TEA (3 equiv.), THF, MW, 100 °C, 10 min, 85%; **(b)** Potassium Phtalimide (0.25 equiv.), DMF, 40 °C, 24 h, 51%; **(c)** 1- $N_2H_4{\cdot}H_2O$ (6 equiv), EtOH, rt, 24 h, 2- NBD-Cl (3 equiv.), MeCN/$NaHCO_{3(sat)}$ (1:1), rt, 2 h, 27%; **(d)** NaN_3 (2 equiv.), DMF, rt, 24 h, 78%; **(e)** $CuSO_4$ (10 mol%), sodium ascorbate (10 mol%), *t*BuOH/H_2O (1:1), 32%.

that retained the necessary structural features contributing to its activity. Amino-NBD (7-amino-4-nitro-2,1,3-benzoxadiazole) was chosen as the fluorophore due to its extensive use as a fluorescent reporter of many metabolites, such as cholesterol (Ramirez et al., 2010), phospholipids (Kol et al., 2003), fatty acids (Pohl et al., 2002) and natural products (Woodland et al., 2017). This moiety was incorporated at the end of the decyl chain to form the fluorescent probe **1-NBD** (Scheme 1).

To assess how the newly designed fluorescent analogue would mimic compound **1**, we considered the most crucial topological descriptors. For this purpose, we calculated logP, topological polar surface area (TPSA) and volume using the Molinspiration platform (Molinspiration Cheminformatics Free Web Services, 2024). LogP showed minimal divergence between the two compounds (**1** = 4.62, **1-NBD** = 5.03), TPSA displayed a notably higher value for **1-NBD** (**1** = 60.26 Å^2, **1-NBD** = 157.04 Å^2), and the volume of for the fluorescent analogue was larger, as expected (**1** = 359.38 Å^3, **1-NBD** = 484.01 Å^3). Despite the differences in volume and TPSA, that are consequence of the NBD located on the aliphatic tail, logP was not considerably affected. To validate the significance of the disparities in calculated topological descriptors of **1** and **1-NBD**, we calculated these properties for previously reported NBD-tagged metabolites that have undergone successful validation through transporter or permease experiments. Specifically, we calculated logP, TPSA and volume for NBD-tagged cholesterol (Song et al., 2015), cholic acids (Májer et al., 2012), glucose (Yoshioka et al., 1996), fructose (Tanasova et al., 2013) and spermidine (Jagu et al., 2019) and compared them to the native metabolites. The results (Table 2, and Supplementary Figures S18–S20) indicated similar or even larger deviations for the reported NBD-tagged metabolites compared to **1** and **1-NBD**. This outcome instilled confidence that the proposed structure could potentially be internalized by a permease. We acknowledge that **1-NBD** violates several Lipinski/Veber thresholds (3 violations; TPSA = 157 Å^2; MW = 528.6) (Table 2). It was nevertheless selected for the uptake-tracing experiments for three converging reasons: (i) appending NBD invariably introduces such excursions in physicochemical space, and the literature-validated NBD analogues used here as benchmarks (NBD-cholesterol, NBD-bile acids, NBD-glucose, NBD-fructose, NBD-spermidine) display deviations of comparable or greater magnitude relative to their parent metabolites yet are still recognised by their cognate transporters; (ii) calculated logP for **1-NBD** (5.03) remains close to that of parent compound **1** (4.62), arguing that overall lipophilicity, the parameter most relevant to membrane partitioning and to interaction with a hydrophobic substrate channel, is largely preserved; and (iii) NBD was placed at the distal end of the alkyl tail, the structural region least implicated in TcAAAP069 recognition by SAR, leaving the proline-triazole pharmacophore intact. **1-NBD** is therefore proposed as a chemical-biology probe for visualising uptake of this scaffold rather than as a faithful pharmacokinetic surrogate of compound **1**.

The proposed fluorescent derivative **1-NBD** offers the advantage of facile synthesis through click chemistry (CuAAC) between *N*-propargyl methyl prolinate **16** and the *N*-NBD-10-azidodecan-1-amine (NBD-azide, **20**). Compound **16** was obtained via microwave-assisted irradiation of methyl prolinate **14** with propargyl bromide **15**, yielding 85%. The NBD-azide **20** was synthesized in 3 steps starting from commercially available 1,10-dibromodecane **17**. The starting material underwent nucleophilic monosubstitution with potassium phthalimide, resulting in 1-phtalimide-10-bromodecane **18** with 51% yield. Then, phtalimide was converted into the free amine using hidrazine, which without further purification acted as nucleophile in an aromatic substitution to NBD-Cl to obtain compound **19** with a two-step yield of 27%.

TABLE 2 Physicochemical parameters of metabolites and their NBD analogues.

Compound	miLogP	TPSA (Å^2)	Volume (Å^3)	MW	natoms	nON	nOHNH	nviolations	nrotb
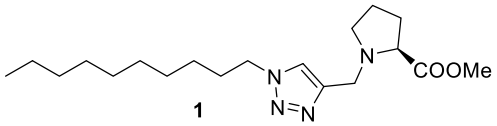 1	4.62	60.26	359.38	350.51	25	6	0	0	13
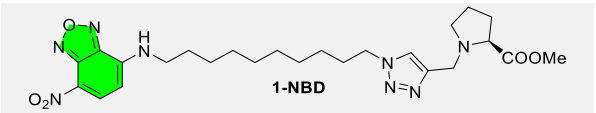 1-NBD	5.03	157.04	484.01	528.61	38	13	1	3	17
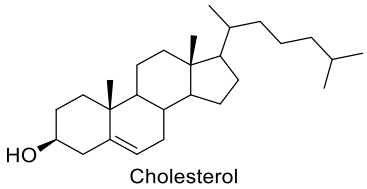 Cholesterol	7.62	20.23	423.13	386.66	28	1	1	1	5
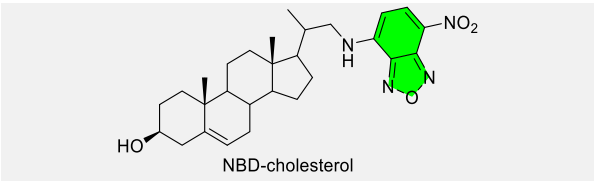 NBD-cholesterol	6.50	117.00	463.97	494.64	36	8	2	1	5
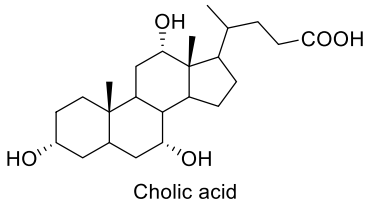 Cholic acid	3.33	97.98	406	408.58	29	5	4	0	4
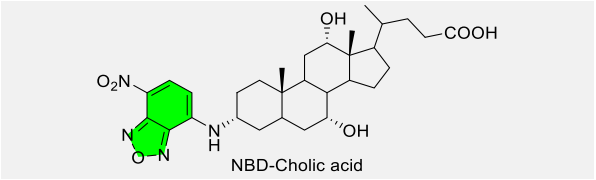 NBD-Cholic acid	5.94	174.53	522	570.69	41	11	4	3	7

(*Continued*)

10.3389/fchbi.2026.1848258

TABLE 2 Continued

Compound	miLogP	TPSA (Å^2)	Volume (Å^3)	MW	natoms	nON	nOHNH	nviolations	nrotb
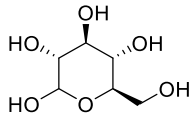 Glucose	−2.64	110.37	151.81	180.16	12	6	5	0	1
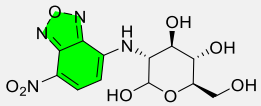 NBD-glucose	−0.26	186.92	268.18	342.26	24	12	5	1	4
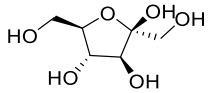 Fructose	−2.04	110.37	151.46	180.16	12	6	5	0	2
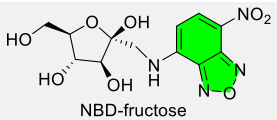 NBD-fructose	−0.10	186.92	267.83	342.26	24	12	5	1	5
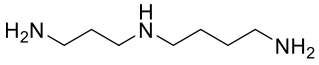 Spermidine	−1.83	64.07	165.23	145.25	10	3	5	0	7
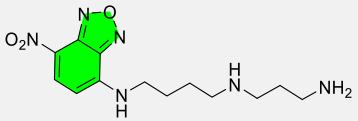 NBD-spermidine	0.67	134.82	278.33	308.34	22	9	4	0	10

10.3389/fchbi.2026.1848258

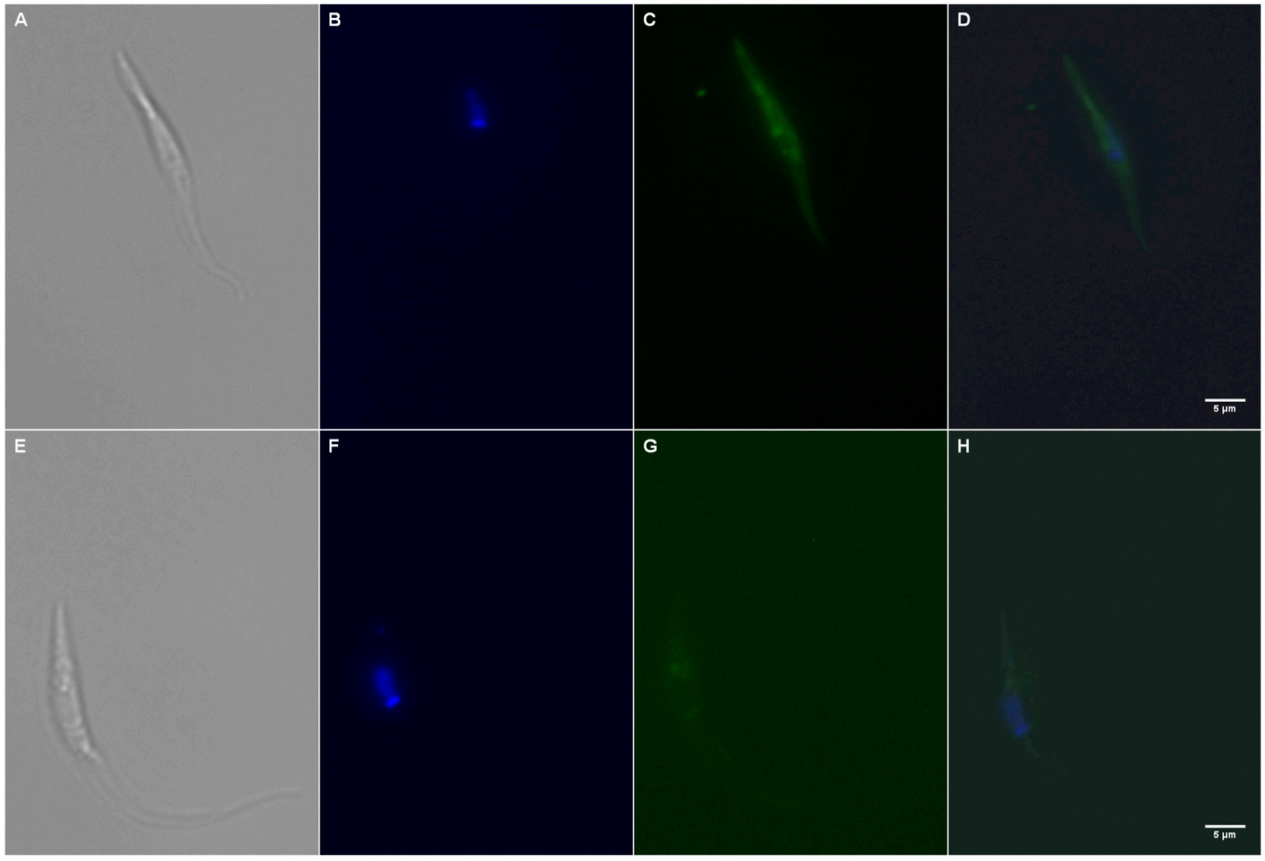

FIGURE 4
Intracellular localization of compound **1-NBD** in epimastigotes of *T. cruzi* (Dm28c). Epimastigotes were incubated during 30 min, at 28 °C with 25 µM of **1-NBD (A–D)**, or with no treatment (Control, **(E–H)**. The uptake and intracellular distribution was assessed by confocal microscopy. **(A, E)** differential interference contrast (DIC) microscopy. **(B, F)** blue channel (DAPI). **(C, G)** green channel: **1-NBD (C)**, Control **(G)**. **(D, H)** merge. The results are representative of at least three independent experiments.

Finally, substitution of the bromine in **19** with sodium azide yielded NBD-azide **20** with a 78% yield (Scheme 1). CuAAC between **16** and **20** provided the final NBD-derivative **1-NBD** with 32% yields (Scheme 1).

UV-vis and fluorescent spectra of compound **1-NBD** were acquired, revealing excitation and emission fluorescence maxima were 472 nm and 538 nm, respectively (see Supplementary Figures S21–S22). After optimizing the detection parameters for compound **1-NBD**, we investigated its incorporation into *T. cruzi* epimastigotes. Parasites were incubated with varying concentrations of the analogue (10–30 µM) for 30 min, and then subjected to confocal microscopy. The best images were obtained for epimastigotes incubated with 25 µM of **1-NBD** (Figure 4).

Analysis of the confocal images showed that the green fluorescent signal of **1-NBD** was concentrated in clusters within the parasite cytoplasm, while being excluded from the plasmatic membrane. This outcome affirms that compound **1-NBD** was internalized either through passive transport across the parasite membrane or via a transporter. The spatial distribution of the fluorescent signal suggested that **1-NBD** could accumulate within internal vesicles.

We emphasise the descriptive nature of this microscopy experiment and outline its current limitations. (i) Uptake was not quantified ratiometrically against an internal reference; the present analysis is therefore qualitative and does not yield concentration- or time-resolved internalisation kinetics. (ii) Untreated parasites imaged in parallel under identical excitation/emission settings showed a very weak signal in the green channel (Figure 4G), characteristic of parasites' autofluorescence, so the intracellular fluorescence in **1-NBD**-treated cells cannot be ascribed to baseline autofluorescence; nevertheless, this control does not rule out probe-induced photophysical artefacts (e.g., NBD trapping in lipid microenvironments unrelated to its parent transporter). (iii) Co-localisation with organelle markers (Mitotracker, LysoTracker, glycosomal/reservosomal markers) was not performed in this study; consequently, the assignment of the cytoplasmic clusters to specific compartments remains tentative. (iv) Critically, microscopy alone cannot establish that internalisation is mediated by TcAAAP069 rather than by passive diffusion or a parallel transport route. We accordingly present these images as visual evidence that the proline-triazole scaffold can enter the parasite.

2.4 SAR study of proline-triazole analogues: Fragment roles in *T. cruzi* inhibition and cytotoxicity

In our previous work, we conducted a Structure–Activity Relationship (SAR) study for proline-1,2,3-triazole analogues

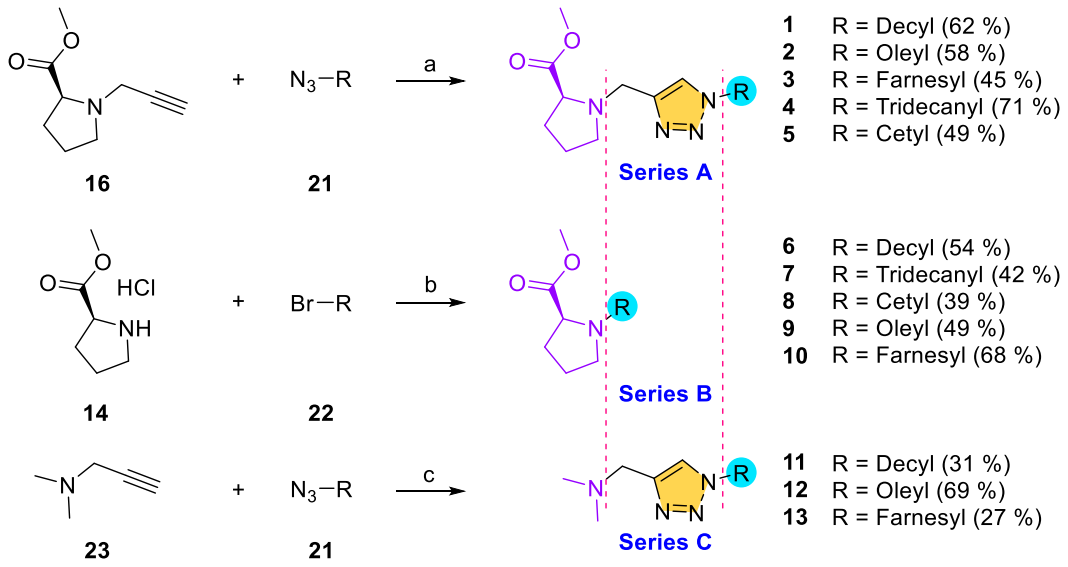

SCHEME 2
Synthesis of Proline analogues studied in this work. **(a)** $CuSO_4$ (10 mol%), sodium ascorbate (10 mol%), *t*BuOH/H_2O (1:1), rt, 24 h; **(b)** DIPEA (3 equiv.), MeCN, rt, 24 h. Isolated yield for each product are in brackets.

(Pro-Trz-R), a family to which compounds **1**, **2** and **3** belong (Fargnoli et al., 2020). In this study, we aimed to expand the SAR to gain a better understanding of the role played by each fragment of the proline analogues under investigation.

Initially, we designed three series of compounds (Scheme 2): **Series A**, comprising Pro-Trz-R analogues (compounds **1** – **5**); **Series B**, where triazole was deleted to form alkyl-proline (Pro-R) analogues (compounds **6** – **10**); and **Series C**, where proline was substituted by a dimethylamine to emulate a truncated version of the amino acid, resulting in dimethylamino-triazole (Me_2N-Trz-R) analogues (compounds **11** – **13**).

Compounds from **Series A** (**1** – **5**) were synthesized via click chemistry by combining *N*-propargyl methyl prolinate **16** and the corresponding alkyl azide **21**, with yields ranging from 45 to 71% (Scheme 2). **Series B** compounds (**6**–**10**) were synthesized through *N*-alkylation of methyl prolinate **14** with the required alkyl bromide **22**, using DIPEA as a base, yielding products at 39–68% (Scheme 2). **Series C** compounds (**11** – **13**) were also prepared through click chemistry, involving *N,N*-dimethylpropargylamine **23** and the appropriate azide **21**, yielding products in 27–69% (Scheme 2).

Subsequently, we conducted an inhibitory activity screening against *T. cruzi* CL14 epimastigotes for compounds **4** – **13** at a fixed concentration of 50 µM (Figure 5). This screening revealed that compounds **4**, **5**, **11**, **12** and **13** exhibited inhibitory effects. IC_{50} values for these compounds were determined (Table 3) through Dose-Response curves, as presented in the (Supplementary Figure S23). Additionally, cytotoxicity against CHO-K_1 cells was assessed for all active compounds, and Selectivity Indexes (SI) were calculated (Table 3).

As previously mentioned, our earlier work (Fargnoli et al., 2020) included an initial SAR study for Pro-Trz-R analogues, which suggested that a chain length of 13–15 carbon atoms a R could improve potency. To confirm this, we synthesized analogues **4** (R = Tridecanyl, -$C_{13}H_{27}$) and **5** (R = Cetyl, -$C_{16}H_{31}$), adding them to compounds **1** (R = Decyl, -$C_{10}H_{21}$), **2** (R = Oleyl) and **3** (R = Farnesyl) in **Series A**. Compound **4** demonstrated the highest potency in this series, with IC_{50} = 27.9 µM, confirming that a chain length of 13 carbon atoms corresponds to a valley of IC_{50} vs. chain length relationship, as previously predicted. Although, when comparing SIs of the saturated aliphatic compounds **1**, **4** and **5**, it is evident that this value is inversely proportional to R chain length, being compound **1** the most selective of the three.

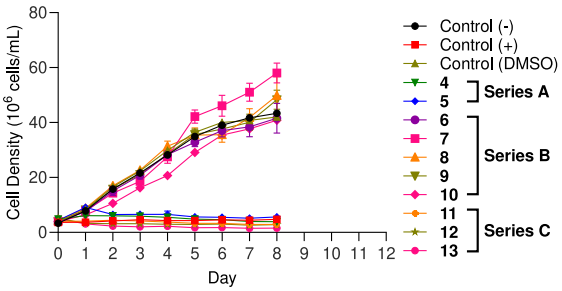

FIGURE 5
Inhibitory activity screening at fixed concentration of 50 µM, against *T. cruzi* CL14 epimastigotes.

To elucidate the role of the triazole moiety in the activity of **Series A**, we synthesized non-triazolic analogues of **Series B** (compounds **6** – **10**), while maintaining the same R groups as in **Series A**, and they were tested against *T. cruzi* CL14 epimastigotes. However, none of these compounds exhibited trypanocidal activity at concentrations up to 50 µM, indicating that the triazole moiety plays a critical role in the anti-*T. cruzi* activity.

Finally, we sought to determine the role of the proline moiety in analogues **1**, **2** and **3**, leading us to design the truncated analogues from **Series C** (compounds **11**, **12** and **13**), while retaining the

TABLE 3 Inhibitory concentration (IC_{50}) determined for compounds 1 - 13 against *T. cruzi* epimastigotes, and cytotoxicity against CHO-K_1 cells.

Series	Compound	R	IC_{50} *T. cruzi* CL14 epimastigotes (μM)[a]	CC_{50} CHO-K_1 cells (μM)[a,b]	SI[c]
A	1	Decyl	39.0 ± 1.4	91.0 ± 2.6	2.3
	2	Oleyl	35.1 ± 7.0	97.0 ± 2.1	2.8
	3	Farnesyl	48.3 ± 1.3	40.4 ± 10.1	0.8
	4	Tridecanyl	27.9 ± 1.6	48.2 ± 4.7	1.7
	5	Cetyl	43.6 ± 5.2	50.3 ± 0.9	1.2
B	6	Decyl	>50	-	-
	7	Tridecanyl	>50	-	-
	8	Cetyl	>50	-	-
	9	Oleyl	>50	-	-
	10	Farnesyl	>50	-	-
C	11	Decyl	32.0 ± 6.9	42.9 ± 6.4	1.3
	12	Oleyl	12.5 ± 1.56	26.0 ± 3.0	2.1
	13	Farnesyl	20.9 ± 2.5	27.1 ± 1.2	1.3
Benznidazole			26.6 ± 4.5 (Fonseca-Berzal et al., 2018)	>200	>7.5

[a]IC_{50}s and CC_{50}s were determined as the average (±SD) of three independent measurements.
[b]- = not measured.
[c]SI = CC_{50} (CHO-K_1)/IC_{50} (*T. cruzi*).

original R groups from **Series A** compounds. Compounds from **Series C** (average IC_{50} = 21.8 μM) displayed greater activity than **Series A** (average IC_{50} = 38.8 μM). Upon comparing the cytotoxic effects of both series against the CHO-K_1 cell line, it became evident that **Series C** (average CC_{50} = 32.0 μM) were more cytotoxic than **Series A** (average CC_{50} = 76.1 μM) (Table 3). Regarding the SIs, compounds **1** vs. **11** and compounds **2** vs. **12** presented a 1.8-fold and a 1.3-fold reduction in selectivity when proline moiety is removed, respectively. Only farnesyl-substituted compounds **3** vs. **13** presented an increment in selectivity with proline removal (1.6-fold), although they are both with SIs close to the unit, indicating that they are antiparasitic and cytotoxic in equal amounts, and differences are not statistically significant. These findings underscore the limited selectivity of the dimethylamine analogues **11** – **13**. More broadly, although the SAR exercise improved potency in some series mammalian selectivity remains limited across the set: SI values for active compounds lie in the 0.8–2.8 range, well below the ≥10 threshold typically considered acceptable for early antiparasitic leads (Kratz, 2019), meaning that further medicinal-chemistry optimisation will be required to widen the therapeutic window. Although, this compound generation proved to be very informative as chemical-biology probes for dissecting proline-transport function.

3 Discussion

The significance of proline in *T. cruzi* metabolism was initially established in the late 1950s (Zeledon, 1960) when the capability of epimastigotes to oxidize this amino acid was first demonstrated. Subsequently, the connection between amino acids consumption and energy metabolism in trypanosomatids was elucidated (Cazzulo, 1994), and it was proposed that enzymes involved in these pathways could serve as potential targets for the development of new chemotherapeutic agents (Silber et al., 2005). This study leverages synthetic proline analogues as chemical probes to dissect the functional significance of proline transport in *T. cruzi*, in order to validate it as a potential drug target.

In this study, we have demonstrated the activity of proline analogues **1**, **2** and **3** against various *T. cruzi* strains representing the six DTUs (Table 1). Interestingly, the strain belonging to TcV was more sensitive to these compounds, while TcVI demonstrated reduced sensitivity to analogue **3**, and TcIV displayed reduced sensitivity to analogue **1**. However, it's essential to note that drawing definitive conclusions from these subtle differences can be challenging. Previous studies have indicated variations in susceptibility to benznidazole among different strains, but current understanding suggests that these differences observed in clinical trials are more likely attributed to environmental factors rather than intrinsic biological distinctions among the strains (Zingales, 2018). Therefore, our tested compounds exhibit consistent broad-spectrum activity against various *T. cruzi* DTUs. While all DTUs are inhibited within a comparable micromolar range, the observed variability highlights inherent biological differences among DTUs, potentially linked to genetic diversity, metabolic adaptations, or differential drug-target interactions. This underscores the challenge of ensuring uniform efficacy across all DTUs during drug development. Compounds should be optimized to overcome strain-specific resistance mechanisms, and preclinical evaluation against representative strains of each DTU is critical to validate pan-

DTU activity, minimizing the risk of incomplete therapeutic coverage in heterogeneous Chagas disease populations.

Our investigation reveals that proline analogues **1**, **2**, and **3** exhibit distinct biological effects on epimastigotes that correlate directly with their previously documented interactions with the proline transporter TcAAAP069 (Sayé et al., 2017). Compounds **1** and **3**, identified as inhibitors of proline uptake, induce a potent trypanostatic effect characterized by cell cycle arrest (Figure 2D). In contrast, compound **2**, which does not interfere with proline transport, triggers apoptotic cell death (Figures 2A–C). This pattern is consistent with chemical interference with proline transport not being immediately lethal but rather imposing a metabolically arrested state, although direct demonstration of target engagement was not performed in the present study. The apparent reversibility of this arrest upon compound washout (Figure 3) further underscores that transport inhibition alone is cytostatic, not cytotoxic, under these conditions. This model system allows us to separate the consequences of proline starvation from generic cellular toxicity, a distinction crucial for understanding the parasite's metabolic network.

The differential potency between transport inhibitors **1** and **3** offers further mechanistic insight. The more rigid, unsaturated farnesyl chain of analogue **3** confers greater inhibitory potency against TcAAAP069 (Sayé et al., 2017) and a more pronounced cell cycle arrest at its IC_{50}, compared to analogue **1**, which required a higher concentration (IC_{80}) for a detectable effect. This suggests that the inhibitor-transporter interaction is highly sensitive to the steric and conformational properties of the substituent. Crucially, the synthesis of a fluorescent derivative of compound **1** confirmed that this transport-competent analogue is internalized by the parasite, localizing in cytoplasmic clusters (Figure 5). This visual evidence is consistent with a model in which these analogues are taken up by the parasite, and is compatible with their previously reported behaviour as competitive substrates of the TcAAAP069 permease (Sayé et al., 2017).

Furthermore, to better comprehend the crucial components responsible for the anti-*T. cruzi* activity in the proline analogues, we conducted a structure-activity relationship (SAR) study. The variations introduced allowed us to categorize the compounds into three series (Scheme 2): **Series A** (Pro-Trz-R), **Series B** (Pro-R) and **Series C** (Me_2N-Trz-R). One key discovery was the confirmation that the chain length of the alkyl group (R) in **Series A** influences the compounds' potency. Specifically, we found that a chain length of 13 carbon atoms (R = tridecanyl, compound **4**) exhibited the highest potency (IC_{50} = 27.90 μM) (Table 3). This result aligns with our previous SAR studies suggesting that a chain length of 13–15 carbon atoms enhances the inhibitory effect (Fargnoli et al., 2020).

The study also aimed to elucidate the role of the triazole moiety in the inhibitory activity. To investigate this, we synthesized the non-triazolic analogues in **Series B** while maintaining the same R groups as in **Series A**. However, none of these compounds exhibited activity (Table 3), indicating that the 1,2,3-triazole moiety plays a critical role in the anti-*T. cruzi* activity. The 1,2,3-triazoles integral components of a wide range of biologically relevant structures and have the capacity to mimic an amide bond, making them biocompatible and highly stable structures (Kolb and Sharpless, 2003; Bonandi et al., 2017). Although 1,2,3-triazoles are mostly used as linkers in biologically active structures, they can also interact with diverse biological targets. Additionally, they are also recognized as pharmacophore components (Agalave et al., 2011; Dheer et al., 2017).

Another critical aspect of the research was to investigate the role of the proline moiety in analogs **1**, **2** and **3**. This led to the design of truncated analogues in **Series C** (compounds **11**, **12** and **13**), while retaining the original R groups from **Series A** compounds. Surprisingly, **Series C** displayed greater inhibitory activity than **Series A** (Table 3). However, it was also observed that **Series C** exhibited a lower selectivity towards mammalian cells than **Series A** (average SI: **Series A** = 2.0, **Series C** = 1.6). The proline moiety, therefore, is not merely a carrier but confers selectivity towards the parasite's proline acquisition machinery. This is further emphasized by comparing analogue **3** to our previously reported triazole-based CYP51 inhibitor (Supplementary Figure S25) (Porta et al., 2017); the simple substitution of a methyl ester for a methyl prolinate shifts the activity profile from targeting ergosterol biosynthesis to inhibiting proline uptake. Thus, the proline-triazole chimera emerges as a specific scaffold for targeting amino acid transport.

The stage-specific activity profile of the proline analogues (potent against epimastigotes but inactive against intracellular amastigotes) is a key finding that underscores a fundamental metabolic reprogramming between the insect and mammalian stages of *T. cruzi*. This dichotomy directly reflects the distinct metabolic demands and environments of each life form. Epimastigotes in the nutrient-variable insect gut prioritize the efficient uptake and catabolism of specific amino acids, with proline serving as a primary carbon and energy source (Alencar et al., 2025). Our results confirm that this stage is exquisitely sensitive to chemical inhibition of its high-affinity proline transporter, TcAAAP069. In stark contrast, upon differentiation to the intracellular amastigote, the parasite undergoes extensive metabolic remodelling to exploit the nutrients from the host cell cytoplasm (Dumoulin and Burleigh, 2021; Liu et al., 2021). Transcriptomic studies indicate that amastigotes upregulate pathways for fatty acid oxidation, amino acid catabolism, and oxidative phosphorylation, shifting away from a dependence on a single amino acid like proline (Liu et al., 2021). Critically, amastigotes exhibit significant metabolic flexibility, retaining the capacity to utilize multiple host-derived carbon sources, including glucose and glutamine (Shah-Simpson et al., 2017; Dumoulin and Burleigh, 2021). This flexibility, a key determinant of parasite persistence, means that inhibiting a single nutrient uptake route (proline transport) is insufficient to compromise amastigote viability, as the parasite can readily switch to alternative fuels (Dumoulin and Burleigh, 2021). Therefore, the inactivity of our proline-targeted probes against amastigotes reveals that proline acquisition via TcAAAP069 may be more relevant for the insect stage than for the mammalian intracellular stage. Several caveats warrant consideration regarding the apparent stage-specific activity of our proline analogues. First, the non-cytotoxic window in the mammalian host-cells: as shown in Table 3, compounds present rather low to moderate CC_{50} values against CHO-K_1. In standard intracellular amastigote assays, host cells must remain viable throughout infection and compound exposure. Consequently, the lack of observed activity against amastigotes may be explained, at

least in part, by compound-induced host cell death or severe cytostasis, which would prevent the normal progression of the intracellular infection rather than reflecting intrinsic resistance of the amastigote stage. Second, even if host cells survive, the amastigote is separated from the extracellular medium by the host plasma membrane and the parasitophorous vacuole membrane, which may impose additional permeability barriers that are not present in axenic epimastigote cultures. Third, the metabolic programming of amastigotes differs substantially from that of epimastigotes; intracellular amastigotes proliferate within the nutrient-rich host cytoplasm and may rely less on exogenous proline uptake, making them less vulnerable to proline transport inhibitors. Finally, we cannot rule out stage-specific differences in compound metabolism, sequestration, or efflux.

In summary, these proline analogues serve as useful chemical-biology probes that have enabled us to establish, in epimastigotes, an association between exposure to compounds **1** and **3** — previously characterised as inhibitors of TcAAAP069-mediated proline uptake—and a reversible G1 cell-cycle arrest, while compound **2** produces an apoptosis-like phenotype consistent with an off-pathway effect. We were also able to define the structural elements (proline core, triazole linker, optimised alkyl chain) essential for this specific activity, and to document a clear stage-dependent activity profile, with potency restricted to the epimastigote form. The present work adds up evidence on the relevance of proline transport in parasites, making it a valuable candidate therapeutic target.

4 Conclusion

This study demonstrates the utility of synthetic proline analogues as valuable chemical biology tools to dissect the functional role of amino acid transport in *Trypanosoma cruzi*. By employing these compounds as chemical probes, we provide chemical-biology evidence consistent with the proline permease TcAAAP069 being a candidate vulnerable node in the metabolism of the insect-stage epimastigote.

The proline analogues **1**, **2** and **3**, have demonstrated broad-spectrum activity against various *T. cruzi* DTUs, making them promising candidates for combating different strains of the parasite. Additionally, the study uncovered distinct modes of action: compound **2** induces apoptotic cell death, while compounds **1** and **3** induce cell cycle arrest. These differences in mechanisms of action align with their effects on proline transport inhibition. The study also provides insights into the internalization of proline analogues, with a fluorescent derivative (**1-NBD**) showing uptake and localization within the parasite cytoplasm, potentially through competition with proline uptake. Furthermore, a structure-activity relationship (SAR) study highlights the importance of the proline-triazole hybrid and the role of the R groups in influencing the compounds' activity and selectivity.

Collectively, this research provides a robust mechanistic framework for understanding proline uptake's role in *T. cruzi*. Future work should leverage this foundation to design next-generation probes with modified pharmacokinetic properties or dual-targeting capabilities to challenge the metabolic plasticity of the amastigote stage.

5 Materials and methods

5.1 Chemistry

Chemical reagents were purchased from commercial suppliers and used without further purification, unless otherwise noted. Column chromatography was performed with silica gel 60 (230–400 mesh). Yields were calculated for material judged homogeneous by thin layer chromatography (TLC) and nuclear magnetic resonance (^{1}H NMR).

^{1}H and ^{13}C NMR spectra were acquired on a Bruker Avance II 300 MHz (75.13 MHz) using $CDCl_3$ as solvent. Chemical shifts (δ) were reported in ppm downfield from tetramethylsilane and coupling constants are in hertz (Hz). NMR spectra were obtained at 298 K unless otherwise stated and samples run as a dilute solution of the stated solvent. All NMR spectra were referenced to the residual undeuterated solvent as an internal reference. The following abbreviations were used to explain the multiplicities: s = singlet, d = doublet, t = triplet, q = quartet, m = multiplet, br = broad. Assignment of proton resonances was confirmed by correlated spectroscopy. Electrospray ionization high-resolution mass spectra (ESI-HRMS) were recorded on a Bruker MicroTOF II.

5.1.1 Synthesis of methyl prop-2-yn-1-yl-L-prolinate (16)

To a solution of methyl prolinate (**14**) 120 mM in THF (anh), NEt_3 (3 equiv.) and 80% propargyl bromide in toluene (**15**) (2 equiv.) were added, and the reaction mixture reacted under microwave irradiation at 100 °C for 10 min. The reaction crude underwent to extraction with ethyl acetate (x3) and water (x3). The combined organic layer was dried over Na_2SO_4 and evaporated. The product was purified by column chromatography in silica gel with increasing hexane/ethyl acetate gradient to yield the expected product as a yellow oil (80%). Spectral data is consistent with the previously reported (Fargnoli et al., 2020).

5.1.2 General procedure for the Cu(I) mediated 1,3-dipolar cycloaddition

The corresponding alkyne (1 equiv.) and azide (1.1 equiv.) were suspended in 10 mL/eq of *t*BuOH:H_2O (1:1), and then 1M $CuSO_4$ solution (0.05 equiv.) and 1M sodium ascorbate solution (0.2 equiv.) were added. The mixture was stirred overnight at room temperature. Brine was added, and the solution was extracted with ethyl acetate. Combined organic extracts were dried over Na_2SO_4 and evaporated. Products were purified by column chromatography in silica gel with increasing hexane/ethyl acetate/methanol gradients.

5.1.3 General procedure for methyl-L-prolinate *N*-alkylation

Methyl *N*-alkyl L-prolinate analogues were synthesized through a modified method by Moore (Moore et al., 2005). **14** (1 equiv.), alkyl chloride (1.1 equiv.) and *N,N*-diisopropylethylamine (3 equiv.) were dissolved in acetonitrile (1 mL/equiv.). The mixture reacted under nitrogen atmosphere at room temperature for 24 h. Afterwards, solvent was evaporated, the reaction mixture was

dissolved in CH_2Cl_2 and it was extracted with CH_2Cl_2/H_2O, washing 3 times each layer. The organic extracts were dried over Na_2SO_4 and evaporated. The *N*-alkyl products were purified by column chromatography in silica gel with increasing hexane/ethyl acetate gradients.

5.1.4 Methyl ((1-decyl-1H-1,2,3-triazol-4-yl) methyl)-L-prolinate (1)

Following the Cu(I) mediated 1,3-dipolar cycloaddition general procedure, compound **1** (Fargnoli et al., 2020) was obtained from alkyne **16** and decyl azide as a yellow oil in 62% yield. ^{1}H NMR (300 MHz, $CDCl_3$) δ 7.50 (s, 1H, C8-H), 4.32 (t, *J* = 7.3 Hz, 2H, C10-H), 4.02 (d, *J* = 13.8 Hz, 1H, C6-Ha), 3.83 (d, *J* = 13.8 Hz, 1H, C6-Hb), 3.70 (s, 3H, C9-H), 3.32 (dd, *J* = 8.9, 6.2 Hz, 1H, C3-H), 3.14 (m, 1H, C2-Ha), 2.54 (q, *J* = 8.3 Hz, 1H, C2-Hb), 2.23 – 1.70 (m, 6H, C1-H, C4-H, C11-H), 1.38 – 1.18 (m, 14H, C12-H, C13-H, C14-H, C15-H, C16-H, C17-H, C18-H), 0.88 (t, *J* = 6.4, 6.4 Hz, 3H, C19-H). ^{13}C NMR (75 MHz, $CDCl_3$) δ 174.5 (C, C5), 144.4 (C, C7), 122.5 (CH, C8), 64.7 (CH, C3), 53.3 (CH_2, C2), 51.9 (CH_3, C9), 50.3 (CH_2, C10), 48.7 (CH_2, C6), 31.8 (CH_2), 30.3 (CH_2), 29.4 (CH_2), 29.4 (CH_2), 29.4 (CH_2, C4), 29.2 (CH_2), 29.0 (CH_2), 26.5 (CH_2), 23.0 (CH_2, C1), 22.6 (CH_2), 14.1 (CH_3, C19). ESI-HRMS m/z $[M + H]^+$ calcd for $C_{19}H_{35}N_4O_2$ 351.2754, found 351.2746.

5.1.5 Methyl (Z)-((1-(octadec-9-en-1-yl)-1H-1,2,3-triazol-4-yl)methyl)-L-prolinate (2)

Following the Cu(I) mediated 1,3-dipolar cycloaddition general procedure, compound **2** (Fargnoli et al., 2020) was obtained from alkyne **16** and oleyl azide as a yellow oil in 58% yield. ^{1}H NMR (300 MHz, $CDCl_3$) δ 7.51 (s, 1H, C8-H), 5.40 – 5-30 (m, 2H, C18-H, C19-H), 4.32 (t, *J* = 7.2 Hz, 2H, C10-H), 4.01 (d, *J* = 13.8 Hz, 1H, C6-Ha), 3.82 (d, *J* = 13.8 Hz, 1H, C6-Hb), 3.69 (s, 3H, C9-H), 3.31 (dd, *J* = 8.9, 6.1 Hz, 1H, C3-H), 3.13 (td, *J* = 9.1, 8.3, 3.0 Hz, 1H, C2-Ha), 2.52 (q, *J* = 8.3 Hz, 1H, C2-Hb), 2.25 – 1.73 (m, 10H, C1-H, C4-H,C11-H, C17-H, C20-H), 1.36 – 1.22 (m, 22H, C12-H, C13-H, C14-H, C15-H, C16-H, C21-H, C22-H, C23-H, C24-H, C25-H, C26-H), 0.88 (t, J = 6.5 Hz, 3H, C27-H). ^{13}C NMR (75 MHz, $CDCl_3$) δ 172.9 (C, C5), 144.5 (C, C7), 130.0(CH, C19), 129.7 (CH, C18), 122.5 (CH, C8), 64.7 (CH, C3), 53.3 (CH_2, C2), 51.9 (CH_3, C9), 50.3 (CH_2, C10), 48.7 (CH_2, C6), 32.6 (CH_2), 31.9 (CH_2), 30.3 (CH_2), 29.7 (CH_2), 29.7 (CH_2), 29.5 (CH_2, C4), 29.4 (CH_2), 29.3 (CH_2), 29.1 (CH_2), 29.0 (CH_2), 27.2 (CH_2), 27.2 (CH_2), 26.5 (CH_2), 23.0 (CH_2, C1), 22.7 (CH_2), 22.6 (CH_2), 14.1 (CH_3, C27). ESI-HRMS m/z $[M + K]^+$ calcd for $C_{27}H_{48}N_4O_2K$ 499.3408, found 499.3412.

5.1.6 Methyl ((1-((2E,6E)-3,7,11-trimethyldodeca-2,6,10-trien-1-yl)-1H-1,2,3-triazol-4-yl)methyl)-L-prolinate (3)

Following the Cu(I) mediated 1,3-dipolar cycloaddition general procedure, compound **3** (Fargnoli et al., 2020) was obtained from alkyne **16** and farnesyl azide as a yellow oil in 45% yield. ^{1}H NMR (300 MHz, $CDCl_3$) δ 7.48 (s, 1H, C8-H), 5.42 (t, *J* = 7.1 Hz, 1H, C11-H), 5.17 – 5.02 (m, 2H, C15-H, C19-H), 4.93 (dd, *J* = 7.3, 1.2 Hz, 2H, C10-H), 4.00 (d, *J* = 13.7 Hz, 1H, C6-Ha), 3.79 (d, *J* = 13.7 Hz, 1H, C6-Hb), 3.70 (s, 3H, C9-H), 3.31 (dd, *J* = 8.9, 6.2 Hz, 1H, C3-H), 3.13 (t, *J* = 8.3 Hz, 1H, C2-Ha), 2.52 (q, *J* = 8.4 Hz, 1H, C2-Hb), 2.25 – 1.73 (m, 15H,C1-H, C4-H, C13-H, C14-H, C17-H, C18-H, C24-H), 1.71 – 1.56 (m, 9H, C21-H, C22-H, C23-H). ^{13}C NMR (75 MHz, $CDCl_3$) δ 174.5 (C, C5), 144.6 (C, C7), 143.1 (C, C12), 136.3 (C, C16), 131.5 (C, C20), 124.1 (CH, C15), 123.0 (CH, C19), 122.0 (CH, C8), 117.8 (CH, C11), 64.8 (CH, C3), 53.3 (CH_2, C2), 51.9 (CH_3, C9), 48.8 (CH_2, C6), 47.7 (CH_2, C10), 39.7 (CH_2), 32.1 (CH_2), 29.4 (CH_2, C4), 26.3 (CH_2), 25.7 (CH_3), 23.5 (CH_3), 23.0 (CH_2, C1), 17.7 (CH_3), 16.0 (CH_3). ESI-HRMS m/z $[M + H]^+$ calcd for $C_{24}H_{39}N_4O_2$ 415.3067, found 415.3067.

5.1.7 Methyl ((1-tridecyl-1H-1,2,3-triazol-4-yl) methyl)-L-prolinate (4)

Following the Cu(I) mediated 1,3-dipolar cycloaddition general procedure, compound **4** was obtained from alkyne **16** and tridecanyl azide as a yellow oil in 71% yield. ^{1}H NMR (300 MHz, $CDCl_3$) δ 7.50 (s, 1H, C8-H), 4.32 (t, *J* = 7.3 Hz, 2H, C10-H), 4.01 (d, *J* = 13.8 Hz, 1H, C6-Ha), 3.82 (d, *J* = 13.8 Hz, 1H, C6-Hb), 3.70 (s, 3H, C9-H), 3.31 (dd, *J* = 8.9, 6.2 Hz, 1H, C3-H), 3.13 (ddd, *J* = 10.0, 7.2, 3.0 Hz, 1H, C2-Ha), 2.53 (q, *J* = 8.4 Hz, 1H, C2-Hb), 2.23 – 1.73 (m, 6H, C1-H, C4-H, C11-H), 1.40 – 1.15 (m, 20H, C12-H, C13-H, C14-H, C15-H, C16-H, C17-H, C18-H, C19-H, C20-H, C21-H), 0.88 (t, *J* = 6.7 Hz, 3H, C22-H). ^{13}C NMR (75 MHz, $CDCl_3$) δ 174.5 (C, C5), 144.5 (C, C7), 122.5 (CH, C8), 64.7 (CH, C3), 53.3 (CH_2, C2), 51.9 (CH_3, C9), 50.3 (CH_2, C10), 48.7 (CH_2, C6), 31.9 (CH_2), 30.3 (CH_2), 29.6 (CH_2), 29.6 (CH_2), 29.6 (CH_2), 29.5 (CH_2), 29.4 (CH_2), 29.4 (CH_2, C4), 29.3 (CH_2), 29.0 (CH_2), 26.5 (CH_2), 23.1 (CH_2, C1), 22.7 (CH_2), 14.1 (CH_3, C22).

5.1.8 Methyl ((1-hexadecyl-1H-1,2,3-triazol-4-yl) methyl)-L-prolinate (5)

Following the Cu(I) mediated 1,3-dipolar cycloaddition general procedure, compound **5** (Fargnoli et al., 2020) was obtained from alkyne **16** and cetyl azide as a white solid in 49% yield. ^{1}H NMR (300 MHz, $CDCl_3$) δ 7.50 (s, 1H, C8-H), 4.32 (t, *J* = 7.3 Hz, 2H, C10-H), 4.01 (d, J = 13.8 Hz, 1H, C6-Ha), 3.82 (d, *J* = 13.8 Hz, 1H, C6-Hb), 3.70 (s, 3H, C9-H), 3.32 (dd, *J* = 8.9, 6.2 Hz, 1H, C3-H), 3.13 (ddd, *J* = 9.5, 7.1, 3.0 Hz, 1H, C2-Ha), 2.53 (q, *J* = 8.3 Hz, 1H, C2-Hb), 2.23 – 1.71 (m, 6H, C1-H, C4-H, C11-H), 1.34 – 1.21 (m, 26H, C12-H, C13-H, C14-H, C15-H, C16-H, C17-H, C18-H, C19-H, C20-H, C21-H, C22-H, C23-H, C24-H), 0.88 (t, *J* = 6.4 Hz, 3H, C25-H). ^{13}C NMR (75 MHz, $CDCl_3$) δ 174.5 (C, C5), 144.5 (C, C7), 122.5 (CH, C8), 64.7 (CH, C3), 53.3 (CH_2, C2), 51.8 (CH_3, C9), 50.3 (CH_2, C10), 48.7 (CH_2, C6), 31.9 (CH_2), 30.3 (CH_2), 29.7 (CH_2), 29.6 (CH_2), 29.6 (CH_2), 29.5 (CH_2), 29.4 (CH_2), 29.4 (CH_2, C4), 29.3 (CH_2), 29.0 (CH_2), 26.5 (CH_2), 23.0 (CH_2, C1), 22.7 (CH_2), 14.1 (CH_3, C25). ESI-HRMS m/z $[M + Na]^+$ calcd for $C_{25}H_{46}N_4O_2Na$ 457.3513, found 457.3512.

5.1.9 Methyl decyl-L-prolinate (6)

Following the *N*-alkylation general procedure, compound **6** was obtained from **14** and bromodecane as a yellow oil in 54% yield. ^{1}H NMR (300 MHz, $CDCl_3$) δ 3.72 (s, 3H, C6-H), 3.26 – 3.08 (m, 2H, C3-H, C7-Ha), 2.64 (dt, J = 11.7, 7.9 Hz, 1H, C2-Ha), 2.44 – 2.25

(m, 2H, C2-Hb, C7-Hb), 2.20 – 1.72 (m, 4H, C1-H, C4-H), 1.49 (m, 2H, C8-H), 1.27 (m, 14H, C9-H, C10-H, C11-H, C12-H, C13-H, C14-H, C15-H), 0.88 (t, J = 6.5 Hz, 3H, C16-H). ^{13}C NMR (75 MHz, $CDCl_3$) δ 174.9 (C, C5), 66.3 (CH, C3), 55.3 (CH_2, C2), 53.6 (CH_2, C7), 51.8 (CH_3, C6), 31.9 (CH_2), 29.6 (CH_2, C4), 29.5 (CH_2), 29.4 (CH_2), 29.3 (CH_2), 28.6 (CH_2), 27.5 (CH_2), 23.1 (CH_2, C1), 22.7 (CH_2), 14.1 (CH_3, C16). ESI-HRMS m/z $[M + Na]^+$ calcd for $C_{16}H_{31}NO_2Na$ 292.2247, found 292.2245.

5.1.10 Methyl tridecyl-L-prolinate (7)

Following the *N*-alkylation general procedure, compound **7** was obtained from **14** and bromotridecane as a yellow oil in 42% yield. ^{1}H NMR (300 MHz, $CDCl_3$) δ 3.73 (s, 3H, C6-H), 3.24 – 3.09 (m, 2H, C3-H, C7-Ha), 2.70 – 2.58 (m, 1H, C2-Ha), 2.41 – 2.26 (m, 2H, C2-Hb, C7-Hb), 2.20 – 1.75 (m, 4H, C1-H, C4-H), 1.49 (t, *J* = 7.3 Hz, 2H, C8-H) 1.37 – 1.18 (m, 20H, C9-H, C10-H, C11-H, C12-H, C13-H, C14-H, C15-H, C16-H, C17-H, C18-H), 0.88 (t, J = 6.6 Hz, 3H, C19-H). ^{13}C NMR (75 MHz, $CDCl_3$) δ 175.0 (C, C5), 66.3 (CH, C3), 55.4 (CH_2, C2), 53.6 (CH_2, C7), 51.9 (CH_3, C6), 31.9 (CH_2), 29.7 (CH_2), 29.7 (CH_2), 29.7 (CH_2), 29.6 (CH_2), 29.6 (CH_2), 29.5 (CH_2), 29.4 (CH_2), 29.4 (CH_2), 28.7 (CH_2), 27.6 (CH_2), 23.2 (CH_2, C1), 22.7 (CH_2), 14.1 (CH_3, C19). ESI-HRMS m/z $[M + Na]^+$ calcd for $C_{19}H_{37}NO_2Na$ 335.2716, found 335.2710.

5.1.11 Methyl hexadecyl-L-prolinate (8)

Following the *N*-alkylation general procedure, compound **8** was obtained from **14** and cetyl bromide as a yellow oil in 39% yield. ^{1}H NMR (300 MHz, $CDCl_3$) δ 3.72 (s, 3H, C6-H), 3.26 – 3.08 (m, 2H, C3-H, C7-Ha), 2.64 (dt, J = 11.7, 8.1 Hz, 1H, C2-Ha), 2.44 – 2.25 (m, 2H, C2-Hb, C7-Hb), 2.20 – 1.72 (m, 4H, C1-H, C4-H), 1.49 (q, J = 7.0 Hz, 2H, C8-H), 1.26 (m, 26H, C9-H, C10-H, C11-H, C12-H, C13-H, C14-H, C15-H, C16-H, C17-H, C18-H, C19-H, C20-H, C21-H), 0.88 (t, J = 6.7 Hz, 3H, C22-H). ^{13}C NMR (75 MHz, $CDCl_3$) δ 174.9 (C, C5), 66.3 (CH, C3), 55.4 (CH_2, C2), 53.6 (CH_2, C7), 51.8 (CH_3, C6), 31.9 (CH_2), 29.7 (CH_2), 29.7 (CH_2), 29.6 (CH_2), 29.6 (CH_2), 29.5 (CH_2), 29.4 (CH_2), 29.4 (CH_2), 28.7 (CH_2), 27.6 (CH_2), 23.2 (CH_2, C1), 22.7 (CH_2), 14.1 (CH_3, C22).

5.1.12 Methyl (Z)-octadec-9-en-1-yl-L-prolinate (9)

Following the *N*-alkylation general procedure, compound **9** was obtained from **14** and oleyl bromide as a yellow oil in 49% yield. ^{1}H NMR (300 MHz, $CDCl_3$) δ 5.46 – 5.25 (m, 2H, C15-H, C16-H), 3.72 (s, 3H, C6-H), 3.25 – 3.07 (m, 2H, C3-H, C7-Ha), 2.64 (dt, J = 11.7, 7.9 Hz, 1H, C2-Ha), 2.43 – 2.25 (m, 2H, C2-Hb, C7-Hb), 2.19 – 1.72 (m, 8H, C1-H, C4-H, C14-H, C17-H), 1.54 – 1.40 (m, 2H, C8-H), 1.39 – 1.20 (m, 22H, C9-H, C10-H, C11-H, C12-H, C13-H, C18-H, C19-H, C20-H, C21-H, C22-H, C23-H), 0.88 (t, J = 6.6 Hz, 3H, C24-H). ^{13}C NMR (75 MHz, $CDCl_3$) δ 175.0 (C, C5), 129.9 (CH, C16), 129.9 (CH, C15), 66.3 (CH, C3), 55.4 (CH_2, C2), 53.6 (CH_2, C7), 51.8 (CH_3, C6), 32.6 (CH_2), 31.9 (CH_2), 29.8 (CH_2), 29.7 (CH_2), 29.7 (CH_2), 29.5 (CH_2, C4), 29.5 (CH_2), 29.5 (CH_2), 29.4 (CH_2), 29.3 (CH_2), 29.3 (CH_2), 28.7 (CH_2), 27.6 (CH_2), 27.2 (CH_2), 23.2 (CH_2, C1), 22.7 (CH_2), 14.1 (CH_3, C24).

5.1.13 Methyl ((2E,6E)-3,7,11-trimethyldodeca-2,6,10-trien-1-yl)-L-prolinate (10)

Following the *N*-alkylation general procedure, compound **10** was obtained from **14** and farnesyl chloride as a yellow oil in 68% yield. ^{1}H NMR (300 MHz, $CDCl_3$) δ 5.31 (t, *J* = 7.1 Hz, 1H, C8-H), 5.16 – 5.04 (m, 2H, C12-H, C16-H), 3.72 (s, 3H, C6-H), 3.36 – 3.04 (m, 4H, C2-Ha, C3-H, C7-H) 2.36 (q, *J* = 8.4 Hz, 1H, C2-Hb), 2.20 – 1.84 (m, 12H, C1-H, C4-H, C10-H, C11-H, C14-H, C15-H), 1.70 – 1.57 (m, 12H, C18-H, C19-H, C20-H, C21-H). ^{13}C NMR (75 MHz, $CDCl_3$) δ 174.8 (C, C5), 138.7 (C, C9), 12, 135.2 (C, C13), 16, 131.3 (C, C17), 20, 124.4 (CH, C12), 19, 124.0 (CH, C16), 15, 120.7 (CH, C8), 11, 65.4 (CH, C3), 53.5 (CH_2, C2), 51.8 (CH_2, C7), 51.7 (CH_3, C6), 39.8 (CH_2), 39.7 (CH_2), 29.5 (CH_2, C4), 26.8 (CH_2), 26.4 (CH_2), 25.7 (CH_3), 23.1 (CH_2, C1), 17.7 (CH_3), 16.4 (CH_3), 16.0 (CH_3).

5.1.14 1-(1-Decyl-1H-1,2,3-triazol-4-yl)-N,N-dimethylmethanamine (11)

Following the Cu(I) mediated 1,3-dipolar cycloaddition general procedure, compound **11** was obtained from N,N-dimethylprop-2-yn-1-amine (**19**) and decyl azide as a yellow oil in 31% yield. ^{1}H NMR (300 MHz, $CDCl_3$) δ 7.50 (s, 1H, C5-H), 4.34 (t, J = 7.2 Hz, 2H, C6-H), 3.63 (s, 2H, C3-H), 2.30 (s, 6H, C1-H, C2-H), 1.89 (t, J = 7.1 Hz, 2H, C7-H), 1.34 – 1.22 (m, 14H, C8-H, C9-H, C10-H, C11-H, C12-H, C13-H, C14-H), 0.88 (t, J = 6.4 Hz, 3H, C15-H). ^{13}C NMR (75 MHz, $CDCl_3$) δ 144.9 (C, C4), 122.3 (CH, C5), 54.4 (CH_2, C3), 50.3 (CH_2, C6), 45.1 (CH_3, C1, C2), 31.8 (CH_2), 30.3 (CH_2), 29.4 (CH_2), 29.4 (CH_2), 29.2 (CH_2), 29.0 (CH_2), 26.5 (CH_2), 22.6 (CH_2), 14.1 (CH_3, C15).

5.1.15 (Z)-N,N-dimethyl-1-(1-(octadec-9-en-1-yl)-1H-1,2,3-triazol-4-yl)methanamine (12)

Following the Cu(I) mediated 1,3-dipolar cycloaddition general procedure, compound **12** was obtained from alkyne **19** and oleyl azide as a yellow oil in 69% yield. ^{1}H NMR (300 MHz, $CDCl_3$) δ 7.46 (s, 1H, C5-H), 5.48 – 5.24 (m, 2H, C14-H, C15-H), 4.33 (t, *J* = 7.2 Hz, 2H, C6-H), 3.61 (s, 2H, C3-H), 2.28 (s, 6H, C1-H, C2-H), 2.11 – 1.81 (m, 6H, C7-H, C13-H, C16-H), 1.35 – 1.22 (m, 22H, C8-H, C9-H, C10-H, C11-H, C12-H, C17-H, C18-H, C19-H, C20-H, C21-H, C22-H), 0.88 (t, *J* = 6.4 Hz, 3H, C23-H). ^{13}C NMR (75 MHz, $CDCl_3$) δ 145.2 (C, C4), 130.0 (CH, C15), 129.7 (CH, C14), 122.1 (CH, C5), 54.5 (CH_2, C3), 50.3 (CH_2, C6), 45.2 (CH_3, C1, C2), 31.9 (CH_2), 30.3 (CH_2), 29.8 (CH_2), 29.7 (CH_2), 29.5 (CH_2), 29.4 (CH_2), 29.3 (CH_2), 29.2 (CH_2), 29.1 (CH_2), 29.0 (CH_2), 27.2 (CH_2), 27.2 (CH_2), 26.5 (CH_2), 22.7 (CH_2), 14.1 (CH_3, C23).

5.1.16 N,N-dimethyl-1-(1-((2E,6E)-3,7,11-trimethyldodeca-2,6,10-trien-1-yl)-1H-1,2,3-triazol-4-yl)methanamine (13)

Following the Cu(I) mediated 1,3-dipolar cycloaddition general procedure, compound **13** was obtained from alkyne **19** and farnesyl azide as a yellow oil in 27% yield. ^{1}H NMR (300 MHz, $CDCl_3$) δ 7.43 (s, 1H, C5-H), 5.43 (t, *J* = 7.3 Hz, 1H, C7-H), 5.13 – 5.03 (m, 2H, C11-H, C15-H), 4.96 (d, *J* = 7.3 Hz, 2H, C6-H), 3.59 (s, 2H, C3-H),

2.28 (s, 6H, C1-H, C2-H), 2.16 – 1.94 (m, 8H, C9-H, C10-H, C13-H, C14-H), 1.78 (s, 3H, C20-H), 1.68 (s, 3H, C19-H), 1.60 (s, 6H, C17-H, C18-H). ^{13}C NMR (75 MHz, $CDCl_3$) δ 145.3 (C, C4), 143.2 (C, C8), 135.8 (C, C12), 131.4 (C, C16), 124.2 (CH, C11), 123.3 (CH, C15), 121.6 (CH, C5), 117.0 (CH, C7), 54.5 (CH_2, C3), 47.8 (CH_2, C6), 45.2 (CH_3, C1, C2), 39.7 (CH_2), 39.4 (CH_2), 26.7 (CH_2), 26.1 (CH_2), 25.7 (CH_3), 17.7 (CH_3), 16.5 (CH_3), 16.0 (CH_3).

5.1.17 Synthesis of 2-(10-bromodecyl)isoindoline-1,3-dione (18)

1,10-dibromodecane **17** (4 equiv.) was dissolved in anhydrous DMF, and potassium phthalimide (1 equiv.) was added to the solution. The reaction was carried out at 40 °C with constant stirring for 24 h. Water was added, and the solution was extracted with DCM. Combined organic extracts were dried over Na_2SO_4 and evaporated. Product was purified by column chromatography in silica gel with increasing hexane/ethyl acetate gradient to yield the expected product **18** as a white solid (51%). Spectral data is consistent with the previously reported (Saez Talens et al., 2020). ^{1}H NMR (300 MHz, $CDCl_3$) δ 7.84 (dd, *J* = 5.4, 3.1 Hz, 2H, C5-H, C8-H), 7.71 (dd, *J* = 5.5, 3.0 Hz, 2H, C6-H, C7-H), 3.74 – 3.61 (m, 2H, C9-H), 3.40 (t, *J* = 6.9 Hz, 2H, C18-H), 1.84 (p, *J* = 6.9 Hz, 2H, C17-H), 1.73 – 1.61 (m, 2H, C10-H), 1.47 – 1.23 (m, 12H, C11-H, C12-H, C13-H, C14-H, C15-H, C16-H). ^{13}C NMR (75 MHz, $CDCl_3$) δ 168.5 (C, C1, C4), 133.8 (CH, C6, C7), 132.2 (C, C2, C3), 123.2 (CH, C5, C8), 38.1 (CH_2, C9), 34.0 (CH_2, C18), 32.8 (CH_2, C17), 29.3 (CH_2), 29.1 (CH_2), 28.7 (CH_2), 28.6 (CH_2), 28.1 (CH_2), 26.8 (CH_2).

5.1.18 Synthesis of N-(10-bromodecyl)-7-nitrobenzo [c][1,2,5]oxadiazol-4-amine (19)

Following the procedure reported by Wu et al. (2007), phtalimide **18** (1 equiv.) was dissolved in dry ethanol, the solution was stirred and hydrazine (6 equiv.) was added. Reaction was stirred for 12 h at room temperature. After reaction completion, the formed solid was removed through filtration, and the volatile components of the solution were removed under reduced pressure. The remaining crude was redissolved in acetonitrile/saturated aqueous $NaHCO_3$ (1:1), the solution was stirred, and a solution of NBD-Cl (1.5 equiv.) in acetonitrile was slowly added. After 1 h of reaction at room temperature, a solution of NBD-Cl (1.5 equiv.) in acetonitrile was again added, and reaction was stirred for another hour. The reaction crude was worked up with DCM and brine. The organic solvent was collected, dried over anhydrous Na_2SO_4 and evaporated under reduced pressure. The product was purified by column chromatography in silica gel eluted with DCM, to yield **19** as an orange oil with 27%. ^{1}H NMR (300 MHz, $CDCl_3$) δ 8.50 (d, *J* = 8.7 Hz, 1H, C3-H), 6.18 (d, *J* = 8.6 Hz, 2H, C2-H), 3.49 (q, *J* = 6.8 Hz, 2H, C7-H), 3.41 (t, *J* = 6.8 Hz, 2H, C16-H), 1.83 (tt, *J* = 14.2, 7.1 Hz, 4H, C8-H, C15-H), 1.49 – 1.28 (m, 12H, C9-H, C10-H, C11-H, C12-H, C13-H, C14-H). ^{13}C NMR (75 MHz, $CDCl_3$) δ 144.3 (C), 143.8(C), 142.9(C), 136.5(CH, C3), 124.0(C), 98.5(CH, C2), 44.0 (CH_2, C7), 34.0 (CH_2, C16), 32.7 (CH_2), 29.7 (CH_2), 29.3 (CH_2), 29.2 (CH_2), 28.7 (CH_2), 28.5 (CH_2), 28.1 (CH_2), 26.9 (CH_2).

5.1.19 Synthesis of N-(10-azidodecyl)-7-nitrobenzo [c][1,2,5]oxadiazol-4-amine (20)

Bromide **19** (1 equiv.) is dissolved in DMF and NaN_3 (1.5 equiv.) is added to the reaction mixture. The reaction took course at room temperature during 24 h. Once the reaction was complete, water was added and the mixture was extracted with DCM. The organic phase was dried over Na_2SO_4 and evaporated under reduced pressure. Azide purification was performed by column chromatography in silica gel eluted with DCM, to yield **20** as an orange oil with 79%. ^{1}H NMR (300 MHz, $CDCl_3$) δ 8.51 (d, *J* = 9.1 Hz, 1H, NBD), 6.18 (d, *J* = 9.1 Hz, 1H, NBD), 3.49 (dd, *J* = 13.2, 6.3 Hz, 2H, C1-H), 3.25 (t, *J* = 6.9, 2H, C10-H), 1.86 – 1.76 (m, 2H), 1.64 – 1.25 (m, 14H). ^{13}C NMR (75 MHz. $CDCl_3$) δ = 144.3 (C), 143.9 (C), 143.8 (C), 136.4 (CH), 124.1 (C), 98.5 (CH), 51.4 (C1), 44.0 (C10), 29.3 (CH_2), 29.2 (CH_2), 29.1 (CH_2), 28.8 (CH_2), 28.6 (CH_2), 28.5 (CH_2), 26.9 (CH_2), 26.7 (CH_2).

5.1.20 Synthesis of methyl ((1-(10-((7-nitrobenzo [c][1,2,5]oxadiazol-4-yl)amino)decyl)-1H-1,2,3-triazol-4-yl)methyl)-L-prolinate (1-NBD)

Following the Cu(I) mediated 1,3-dipolar cycloaddition general procedure, compound **1-NBD** was obtained from alkyne **16** and azide **20** as an orange solid in 32% yield. ^{1}H NMR (300 MHz, $CDCl_3$) δ 8.50 (d, *J* = 9.1 Hz, 1H, NBD), 7.51 (s, 1H, C7-H), 6.18 (d, *J* = 9.1 Hz, 1H, NBD), 4.33 (t, *J* = 7.2 Hz, 2H, C8-H), 4.01 (d, *J* = 13.8 Hz, C6-H, 1H), 3.82 (d, *J* = 13.8 Hz, 1H, C6-H), 3.69 (s, 3H, OMe), 3.50 (dd, *J* = 8.5, 5.7 Hz, C17-H, 2H), 3.34 – 3.29 (m, 1H, C2), 3.16 – 3.11 (m, 1H, C5), 2.54 – 2.51 (m, 1H, C5), 2.00 – 1.67 (m, 6H), 1.30 (s, 14H). ^{13}C NMR (75 MHz, $CDCl_3$) δ 174.5 (C=O), 144.7 (C), 144.3 (C), 143.9 (C), 136.8 (=C-H), 123.5 (C), 122.7 (C7), 98.5 (=C-H), 64.8 (C2), 53.4 (C5), 51.9 (OMe), 50.2 (CH_2), 48.8 (C6), 44.0 (CH_2), 30.1 (C3), 29.4 (CH_2), 29.0 (CH_2), 28.9(CH_2), 28.7 (CH_2), 28.7 (CH_2), 28.4 (CH_2), 28.4 (CH_2), 26.8 (CH_2), 26.2 (CH_2), 23.1 (CH_2).

5.2 Microorganisms and growth conditions of *Trypanosoma cruzi*

T. cruzi strains employed: Sylvio and Dm28c (DTU TcI), Y (DTU TcII), M6241 (DTU TcIII), Can III (DTU TcIV), 92:80 (DTU TcV), CL14 (DTU TcVI).

T. cruzi epimastigotes were maintained in exponential proliferation phase by successive passages (every 48 h) in LIT medium (liver infusion 5 g/L, tryptose 5 g/L, NaCl 4 g/L, KCl 0.4 g/L, Na_2HPO_4 8 g/L, hemin 10 mg/L, supplemented with 10% fetal bovine serum and glucose at a final concentration of 0.2%, pH 7.2) (Camargo, 1964), at 28 °C and 5% CO_2 except otherwise specified.

5.3 Proliferation and IC_{50} determination in *T. cruzi* epimastigotes

Exponentially proliferating *T. cruzi* epimastigotes (2.5×10^6 cells/mL) were seeded in 96-well plates and further treated with different concentrations of each analogue (concentration range from 25 to 250 μM) or untreated (negative control). As a positive

control, a combination of rotenone (60 μM) and antimycin (0.5 μM) was used. The plates were incubated at 28 °C for 8–10 days. Cell proliferation was spectrophotometrically measured by recording the absorbance at 620 nm every 24 h for 8–10 days as described by Magdaleno et al. (2009) The absorbance was transformed into cell density values (cells/mL) using a linear regression equation that was previously obtained under the same conditions. Data from the mid-exponential growth phase were used to determine the concentration of the analogues that inhibited 50% of the parasite proliferation (IC_{50}). For this, we explored classic dose-response sigmoid functions to find the best fit to the obtained data (Magdaleno et al., 2009). Each experiment was made in triplicates, and the results presented correspond to the average of three independent experiments.

5.4 Effect of compounds on mammalian cell viability

Chinese hamster ovary cell line (CHO-K_1) 1.0×10^5 cells/well were seeded in 96-well plate, 100 μL final volume in RPMI medium supplemented with FCS (10%) in the presence of different concentrations of compounds (200 – 3.125 μM). Cells without treatment were used as control. After 72 h, the cell viability was assessed by resazurin assay as previously described (Cuevas-Hernández et al., 2021). The cells were incubated in the presence of 0.125 μg/μL resazurin for 3 h at 37 °C in the absence of light. The fluoresce signal was measured in a Spectra Max M3 fluorometer (Molecular devices) at λ_{exc} 560 nm and λ_{em} 590 nm.

5.5 Washout of compounds

Exponentially proliferating epimastigotes were maintained in LIT medium and treated with the IC_{50} or IC_{80} of compounds **1**, **2** and **3** for 48 h. Then, the parasites were washed once in PBS and resuspended in LIT medium, at the same initial concentration of parasites, without treatment. Then, the parasites were seeded in 96-well plate and kept at 28 °C. The proliferation was followed up spectrophotometrically, as described previously. Cell death and cell cycle were analysed 48 h after washout the treatment as described in the next sections.

5.6 Cell death mechanism

T. cruzi, strain CL14 epimastigotes (2.5×10^6 cells/mL) were cultured in LIT medium at 28 °C and treated with compounds **1**, **2** and **3** at their respective IC_{50} or IC_{80} concentration. After 24, 48 and 72 h of incubation, treated cells and controls (1×10^6 cells/mL) were washed once with annexin buffer (10 mM HEPES, 140 mM NaCl and 2.5 mM $CaCl_2$, pH 7.4) and resuspended in 50 μL of the same buffer. The parasites were incubated in ice (protected from light), for 15 min, in the presence of annexin-V FITC (Invitrogen, Eugene, Oregon, United States), according to the manufacturer's instructions, and 1 μg/mL propidium iodide. Then, 450 μL of annexin buffer was added, and the parasites were analysed by flow cytometry (Accuri C6 Plus cytometer, BD Biosciences), with 10,000 events collected and analysed using Flowjo_v10.8.1 software (Jimenez et al., 2008).

5.7 Cell cycle analysis

Epimastigote forms were cultivated in LIT medium and treated with IC_{50} or IC_{80} of the compounds **1**, **2** and **3** during 24, 48 and 72 h. To analyse the DNA content, the parasites were washed once in PBS and resuspended in lysis buffer (phosphate buffer Na_2HPO_4 7.7 mM, KH_2PO_4 2.3 mM, pH 7.4) and digitonin 64 μM. Then, the parasites were incubated in ice for 30 min, and propidium iodide 20 μg/mL was added. The parasites were analysed by flow cytometry (Accuri C6 Plus cytometer, BD Biosciences), with 10,000 events collected and analysed using Flowjo_v10.8.1 software.

5.8 Confocal microscopy

T. cruzi, strain Dm28c epimastigotes (1 mL, 10^7 cells) were incubated with 25 μM of compound **1-NBD**, or without treatment (control), for 30 min at room temperature. Then, supernatant was discarded, and cells were resuspended in PBS and incubated with DAPI for 5 min (5 μg/mL). Afterwards, cells were washed twice with PBS and resuspended in 500 μL of PBS. A 1:5 dilution was done to acquire images. All images were acquired with an Invitrogen Evos M5000 fluorescence microscope. The emission of the samples displaying green fluorescence (treated with **1-NBD**) was registered at 490/535 nm under Argon laser excitation (488 nm). The emission of the samples treated with DAPI was registered at 430/450 nm under laser excitation (405 nm) (Merli et al., 2016). All the images were processed using the ImageJ software (Schneider et al., 2012).

5.9 Statistical analysis

All quantitative experiments were performed as 3 independent biological replicates, each measured in technical triplicate. Data are reported as mean ± SD unless otherwise indicated. IC_{50} and CC_{50} values were obtained by non-linear regression of the log (inhibitor)-vs-response (variable slope, four-parameter) model in GraphPad Prism 10. Statistical comparisons of compound-treated parasites against the matched untreated control (cell-death, cell-cycle, and washout-recovery assays) were performed by two-way ANOVA followed by Šidák's post-hoc multiple-comparisons test at the 95% confidence level (GraphPad Prism 10); significance is reported as *: $0.01 \leq p < 0.05$; **: $0.001 \leq p < 0.01$; ***: $0.0001 \leq p < 0.001$; ****: $p < 0.0001$.

6 Author summary

Chagas disease, caused by the parasite *T. cruzi*, is a significant public health issue in the Americas. The amino acid proline is essential for the parasite's survival, proliferation, and infection. Our study explored proline analogues that inhibit proline uptake by *T. cruzi*. We tested decyl-, oleyl-, and farnesyl-substituted proline analogues on various *T. cruzi* strains and analysed their effects on cell death and the cell cycle. One analogue was tagged with a fluorescent marker to trace its uptake and localization in the parasite. Our findings revealed that the analogues which effect is linked to proline transport led to cell cycle arrest, while the analogue with action non-related to proline transport caused programmed

cell death in *T. cruzi*. Structure-Activity analysis indicated that the combination of proline and triazole is crucial for their activity, while maintaining selectivity. These findings contribute to a deeper understanding of the role of proline uptake and metabolism in *T. cruzi*'s survival.

Data availability statement

The datasets presented in this study can be found in online repositories. The data, including new compound characterization data (NMR, UV-Vis, and chemoinformatics data), Trypanosoma cruzi growth curves (IC_{50} and washout experiments), and cell death experiments (flow cytometry), are available in the Universidad Nacional de Rosario Data Repository under Labadie et al. (2024).

Author contributions

MB: Data curation, Conceptualization, Investigation, Methodology, Writing – original draft, Writing – review and editing, Formal Analysis. FD: Writing – review and editing, Formal Analysis, Data curation, Investigation, Conceptualization, Methodology. MM: Methodology, Writing – review and editing, Investigation, Conceptualization, Formal Analysis, Data curation. LF: Methodology, Writing – review and editing, Data curation, Investigation. LP: Investigation, Data curation, Writing – review and editing. JC: Funding acquisition, Resources, Writing – review and editing, Methodology, Conceptualization, Supervision. AS: Writing – review and editing, Resources, Formal Analysis, Funding acquisition, Methodology, Supervision, Conceptualization. GL: Funding acquisition, Resources, Formal Analysis, Supervision, Writing – review and editing, Methodology, Conceptualization, Writing – original draft.

Funding

The author(s) declared that financial support was received for this work and/or its publication. This work was supported in part by grants from the National Research Council of Argentina, CONICET (CONICET, PIP 2021-2023 11220200101045CO to GL); Agencia Nacional de Promoción Científica y Tecnológica, ANPCyT-Argentina (ANPCyT PICT 2021-I-A-00512 awarded to GL); UNR (Universidad Nacional de Rosario 80020190300101UR), Fundação de Amparo à Pesquisa do Estado de São Paulo grants 2021/12938-0 (awarded to AS) and Conselho Nacional de Pesquisas Científicas e Tecnológicas (CNPq) grant 307487/2021-0 (awarded to AS). The research leading to these results has, in part, received funding from the United Kingdom Research and Innovation via the Global Challenges Research Fund under grant agreement A Global Network for Neglected Tropical Diseases grant number MR/P027989/1. GL and JC are members of the Research Career of the Consejo Nacional de Investigaciones Científicas y Técnicas of Argentina (CONICET). MB, LF, and LP thanks CONICET for the award of a Fellowship.

Conflict of interest

The author(s) declared that this work was conducted in the absence of any commercial or financial relationships that could be construed as a potential conflict of interest.

Generative AI statement

The author(s) declared that generative AI was not used in the creation of this manuscript.

Any alternative text (alt text) provided alongside figures in this article has been generated by Frontiers with the support of artificial intelligence and reasonable efforts have been made to ensure accuracy, including review by the authors wherever possible. If you identify any issues, please contact us.

Publisher's note

Supplementary material

The Supplementary Material for this article can be found online at: https://www.frontiersin.org/articles/10.3389/fchbi.2026.1848258/full#supplementary-material

References

Agalave, S. G., Maujan, S. R., and Pore, V. S. (2011). Click chemistry: 1,2,3-triazoles as pharmacophores. *Chem. Asian J.* 6, 2696–2718. doi:10.1002/asia.201100432

Alencar, M. B., Marsiccobetre, S., Mengarda, A. C., Ballari, M. S., and Silber, A. M. (2025). Energy metabolism in trypanosoma cruzi: the validated and putative bioenergetic and carbon sources. *mBio* 16, e02215-24. doi:10.1128/mbio.02215-24

Barisón, M. J., Rapado, L. N., Merino, E. F., Pral, E. M. F., Mantilla, B. S., Marchese, L., et al. (2017). Metabolomics profiling reveals a finely tuned, starvationinduced metabolic switch in Trypanosoma cruzi epimastigotes. *J. Biol. Chem.* 292, 8964–8977. doi:10.1074/jbc.M117.778522

Barros-Álvarez, X., Cáceres, A. J., Michels, P. A. M., Concepción, J. L., and Quiñones, W. (2014). The phosphoglycerate kinase isoenzymes have distinct roles in the regulation of carbohydrate metabolism in Trypanosoma cruzi. *Exp. Parasitol.* 143, 39–47. doi:10.1016/j.exppara.2014.05.010

Bermudez, J., Davies, C., Simonazzi, A., Pablo Real, J., and Palma, S. (2016). Current drug therapy and pharmaceutical challenges for chagas disease. *Acta Trop.* 156, 1–16. doi:10.1016/j.actatropica.2015.12.017

Bonandi, E., Christodoulou, M. S., Fumagalli, G., Perdicchia, D., Rastelli, G., and Passarella, D. (2017). The 1,2,3-triazole ring as a bioisostere in medicinal chemistry. *Drug Discov. Today* 22, 1572–1581. doi:10.1016/j.drudis.2017.05.014

Bouvier, L. A., Silber, A. M., Galvão Lopes, C., Canepa, G. E., Miranda, M. R., Tonelli, R. R., et al. (2004). Post genomic analysis of permeases from the amino acid/auxin family in

protozoan parasites. *Biochem. Biophys. Res. Commun.* 321, 547–556. doi:10.1016/j.bbrc.2004.07.002

Camargo, E. P. (1964). Growth and differentiation in trypanosoma cruzi. I. Origin of metacyclic trypanosomes in liquid media. *Rev. Inst. Med. Trop. Sao Paulo* 6, 93–100.

Campbell, D. A., Westenberger, S. J., and Sturm, N. R. (2004). The determinants of chagas disease: connecting parasite and host genetics. *Curr. Mol. Med.* 4, 549–562. doi:10.2174/1566524043360249

Cazzulo, J. J. (1994). Intermediate metabolism in Trypanosoma cruzi. *J. Bioenerg. Biomembr.* 26, 157–165. doi:10.1007/978-1-4899-1651-8_7

Contreras, V. T., Salles, J. M., Thomas, N., Morel, C. M., and Goldenberg, S. (1985). *In vitro* differentiation of Trypanosoma cruzi under chemically defined conditions. *Mol. Biochem. Parasitol.* 16, 315–327. doi:10.1016/0166-6851(85)90073-8

Cuevas-Hernández, R. I., Girard, R. M. B. M., Krstulović, L., Bajić, M., and Silber, A. M. (2021). An aromatic imidazoline derived from chloroquinoline triggers cell cycle arrest and inhibits with high selectivity the Trypanosoma cruzi Mammalian host-cells infection. *PLoS Negl. Trop. Dis.* 15, e0009994. doi:10.1371/journal.pntd.0009994

De Souza, W. (2002). From the cell biology to the development of new chemotherapeutic approaches against trypanosomatids: dreams and reality. *Kinetoplastid Biol. Dis.* 1, 1–21. doi:10.1186/1475-9292-1-3

Dheer, D., Singh, V., and Shankar, R. (2017). Medicinal attributes of 1,2,3-triazoles: current developments. *Bioorg. Chem.* 71, 30–54. doi:10.1016/j.bioorg.2017.01.010

Dumoulin, P. C., and Burleigh, B. A. (2021). Metabolic flexibility in Trypanosoma cruzi amastigotes: implications for persistence and drug sensitivity. *Curr. Opin. Microbiol.* 63, 244–249. doi:10.1016/j.mib.2021.07.017

Duschak, V. G. (2019). Major kinds of drug targets in chagas disease or American trypanosomiasis. *Curr. Drug Targets* 20, 1203–1216. doi:10.2174/1389450120666190423160804

Fargnoli, L., Panozzo-Zénere, E., Pagura, L., Barisón, M. J., Cricco, J. A., Silber, A. M., et al. (2020). Targeting L-proline uptake as new strategy for anti-chagas drug development. *Front. Chem.* 8, 696. doi:10.3389/fchem.2020.00696

Fonseca-Berzal, C., Ibáñez-Escribano, A., Vela, N., Cumella, J., Nogal-Ruiz, J. J., Escario, J. A., et al. (2018). Antichagasic, leishmanicidal, and trichomonacidal activity of 2-Benzyl-5-nitroindazole-Derived amines. *ChemMedChem* 13, 1246–1259. doi:10.1002/cmdc.201800084

Jagu, E., Pomel, S., Pethe, S., Cintrat, J. C., Loiseau, P. M., and Labruère, R. (2019). Spermine-NBD as fluorescent probe for studies of the polyamine transport system in Leishmania donovani. *Bioorg. Med. Chem. Lett.* 29, 1710–1713. doi:10.1016/j.bmcl.2019.05.030

Jimenez, V., Paredes, R., Sosa, M. A., and Galanti, N. (2008). Natural programmed cell death in T. cruzi epimastigotes maintained in axenic cultures. *J. Cell. Biochem.* 105, 688–698. doi:10.1002/jcb.21864

Kol, M. A., Van Dalen, A., De Kroon, A. I. P. M., and De Kruijff, B. (2003). Translocation of phospholipids is facilitated by a subset of membrane-spanning proteins of the bacterial cytoplasmic membrane. *J. Biol. Chem.* 278, 24586–24593. doi:10.1074/jbc.M301875200

Kolb, H. C., and Sharpless, K. B. (2003). The growing impact of click chemistry on drug discovery. *Drug Discov. Today* 8, 1128–1137. doi:10.1016/s1936-7961(08)00219-4

Kratz, J. M. (2019). Drug discovery for chagas disease: a viewpoint. *Acta Trop.* 198, 105107–105112. doi:10.1016/j.actatropica.2019.105107

Labadie, G., Ballari, M. S., Damasceno, F. S., Fargnoli, L., Pagura, L., Cricco, J. A., et al. (2024). Data from: Amino Acids metabolism as drug target for anti-trypanosomatids drug discovery. RDA UNR. doi:10.57715/UNR/AXNGVK

Lages-Silva, E., Crema, E., Ramirez, L. E., Macedo, A. M., Pena, S. D., and Chiari, E. (2001). Relationship between Trypanosoma cruzi and human chagasic megaesophagus: blood and tissue parasitism. *Am. J. Trop. Med. Hyg.* 65, 435–441. doi:10.4269/ajtmh.2001.65.435

Liu, Z., Ulrich vonBargen, R., and McCall, L. I. (2021). Central role of metabolism in Trypanosoma cruzi tropism and chagas disease pathogenesis. *Curr. Opin. Microbiol.* 63, 204–209. doi:10.1016/j.mib.2021.07.015

Magdaleno, A., Ahn, I.-Y., Silva Paes, L., and Silber, A. M. (2009). Actions of a proline analogue, L-thiazolidine-4-carboxylic acid (T4C), on Trypanosoma cruzi. *PLoS One* 4, e4534. doi:10.1371/journal.pone.0004534

Májer, F., Salomon, J. J., Sharma, R., Etzbach, S. V., Najib, M. N. M., Keaveny, R., et al. (2012). New fluorescent bile acids: synthesis, chemical characterization, and disastereoselective uptake by Caco-2 cells of 3-deoxy 3-NBD-amino deoxycholic and ursodeoxycholic acid. *Bioorg. Med. Chem.* 20, 1767–1778. doi:10.1016/j.bmc.2012.01.002

Mantilla, B. S., Paes, L. S., Pral, E. M. F., Martil, D. E., Thiemann, O. H., Fernández-Silva, P., et al. (2015). Role of Δ1-pyrroline-5-carboxylate dehydrogenase supports mitochondrial metabolism and host-cell invasion of Trypanosoma cruzi. *J. Biol. Chem.* 290, 7767–7790. doi:10.1074/jbc.M114.574525

Mantilla, B. S., Marchese, L., Casas-Sánchez, A., Dyer, N. A., Ejeh, N., Biran, M., et al. (2017). Proline metabolism is essential for Trypanosoma brucei brucei survival in the tsetse vector. *PLoS Pathog.* 13, 1–29. doi:10.1371/journal.ppat.1006158

Marchese, L., Olavarria, K., Mantilla, B. S., Avila, C. C., Souza, R. O. O., Damasceno, F. S., et al. (2020). Trypanosoma cruzi synthesizes proline *via* a Δ1-pyrroline-5-carboxylate reductase whose activity is fine-tuned by NADPH cytosolic pools. *Biochem. J.* 477, 1827–1845. doi:10.1042/BCJ20200232

Martins, R. M., Covarrubias, C., Galvez Rojas, R., Silber, A. M., and Yoshida, N. (2009). Use of L-proline and ATP production by Trypanosoma cruzi metacyclic forms as requirements for host cell invasion. *Infect. Immun.* 77, 3023–3032. doi:10.1128/IAI.00138-09

Merli, M. L., Pagura, L., Hernández, J., Barisón, M. J., Pral, E. M. F., Silber, A. M., et al. (2016). The Trypanosoma cruzi protein TcHTE is critical for heme uptake. *PLoS Negl. Trop. Dis.* 10, 1–18. doi:10.1371/journal.pntd.0004359

Miles, M. A., Llewellyn, M. S., Lewis, M. D., Yeo, M., Baleela, R., Fitzpatrick, S., et al. (2009). The molecular epidemiology and phylogeography of Trypanosoma cruzi and parallel research on leishmania: looking back and to the future. *Parasitology* 136, 1509–1528. doi:10.1017/S0031182009990977

Molinspiration Cheminformatics free web services (2024). Molinspiration cheminformatics free web services. Available online at: http://www.molinspiration.com (Accessed April 10, 2025).

Moore, J. L., Taylor, S. M., and Soloshonok, V. A. (2005). An efficient and operationally convenient general synthesis of tertiary amines by direct alkylation of secondary amines with alkyl halides in the presence of Huenig's base. *Arkivoc* 2005, 287–292. doi:10.3998/ark.5550190.0006.624

Nowicki, C., and Cazzulo, J. J. (2008). Aromatic amino acid catabolism in trypanosomatids. *Comp. Biochem. Physiol. A Mol. Integr. Physiol.* 151, 381–390. doi:10.1016/j.cbpa.2007.03.010

Oliveira Souza, R. O., Damasceno, F. S., Marsiccobetre, S., Biran, M., Murata, G., Curi, R., et al. (2021). Fatty acid oxidation participates in resistance to nutrient-depleted environments in the insect stages of Trypanosoma cruzi. *PLoS Pathog*, 17, e1009495. doi:10.1371/journal.ppat.1009495

Paes, L. S., Mantilla, B. S., Menezes Zimbres, F., Furusho Pral, E. M., Diogo de Melo, P., Tahara, E. B., et al. (2013). Proline dehydrogenase regulates redox state and respiratory metabolism in Trypanosoma cruzi. *PLoS One* 8, e69419. doi:10.1371/journal.pone.0069419

Pohl, J., Ring, A., and Stremmel, W. (2002). Uptake of long-chain fatty acids in HepG2 cells involves caveolae: analysis of a novel pathway. *J. Lipid Res.* 43, 1390–1399. doi:10.1194/jlr.M100404-JLR200

Porta, E. O. J., Jäger, S. N., Nocito, I., Lepesheva, G. I., Serra, E. C., Tekwani, B. L., et al. (2017). Antitrypanosomal and antileishmanial activity of prenyl-1,2,3-triazoles. *Medchemcomm* 8, 1015–1021. doi:10.1039/c7md00008a

Ramirez, D. M. C., Ogilvie, W. W., and Johnston, L. J. (2010). NBD-Cholesterol probes to track cholesterol distribution in model membranes. *Biochim. Biophys. Acta Biomembr.* 1798, 558–568. doi:10.1016/j.bbamem.2009.12.005

Saez Talens, V., Davis, J., Wu, C. H., Wen, Z., Lauria, F., Gupta, K. B. S. S., et al. (2020). Thiosquaramide-based supramolecular polymers: aromaticity gain in a switched mode of self-assembly. *J. Am. Chem. Soc.* 142, 19907–19916. doi:10.1021/jacs.0c02081

Saye, M., Miranda, M. R., Girolamo, F.D., De Los Milagros Cámara, M., and Pereira, C. A. (2014). Proline modulates the Trypanosoma cruzi resistance to reactive oxygen species and drugs through a novel D, L-Proline transporter. *PLoS One* 9, e92028. doi:10.1371/journal.pone.0092028

Sayé, M., Fargnoli, L., Reigada, C., Labadie, G. R., and Pereira, C. A. (2017). Evaluation of proline analogs as trypanocidal agents through the inhibition of a Trypanosoma cruzi proline transporter. *BBA - General Subj.* 1861, 2913–2921. doi:10.1016/j.bbagen.2017.08.015

Schneider, C. A., Rasband, W. S., and Eliceiri, K. W. (2012). NIH image to ImageJ: 25 years of image analysis. *Nat. Methods* 9, 671–675. doi:10.1038/nmeth.2089

Shah-Simpson, S., Lentini, G., Dumoulin, P. C., and Burleigh, B. A. (2017). Modulation of host central carbon metabolism and *in situ* glucose uptake by intracellular Trypanosoma cruzi amastigotes. *PLoS Pathog.* 13, e1006747. doi:10.1371/journal.ppat.1006747

Silber, A. M., Tonelli, R. R., Martinelli, M., Colli, W., and Alves, M. J. M. (2002). Active transport of L-proline in Trypanosoma cruzi. *J. Eukaryot. Microbiol.* 49, 441–446. doi:10.1111/j.1550-7408.2002.tb00225.x

Silber, A. M., Colli, W., Ulrich, H., Manso Alves, M. J., and Pereira, C. A. (2005). Amino acid metabolic routes in trypanosoma cruzi: possible therapeutic targets against chagas' disease. *Curr. Drug Targets Infect. Disord.* 5, 53–64. doi:10.2174/1568005053174636

Silber, A. M., Tonelli, R. R., Lopes, C. G., Cunha-e-Silva, N., Torrecilhas, A. C. T., Schumacher, R. I., et al. (2009). Glucose uptake in the Mammalian stages of Trypanosoma cruzi. *Mol. Biochem. Parasitol.* 168, 102–108. doi:10.1016/j.molbiopara.2009.07.006

Song, W., Wang, W., Wang, Y., Dou, L., Chen, L., and Yan, X. (2015). Characterization of fluorescent NBD-Cholesterol efflux in THP-1-derived macrophages. *Mol. Med. Rep.* 12, 5989–5996. doi:10.3892/mmr.2015.4154

Sylvester, D., and Krassner, S. M. (1976). Proline metabolism in Trypanosoma cruzi epimastigotes. *Comp. Biochem. Physiology Part B Comp. Biochem.* 55, 443–447. doi:10.1016/0305-0491(76)90318-7

Tanasova, M., Plutschack, M., Muroski, M. E., Sturla, S. J., Strouse, G. F., and Mcquade, D. T. (2013). Fluorescent THF-based fructose analogue exhibits fructose-dependent uptake. *ChemBioChem* 14, 1263–1270. doi:10.1002/cbic.201300164

Tonelli, R. R., Ariel, M., Almeida-de-Faria, M., Hirata, I. Y., Colli, W., and Alves, M. J. M. (2004). L-Proline is essential for the intracellular differentiation of Trypanosoma cruzi. *Cell. Microbiol.* 6, 733–741. doi:10.1111/j.1462-5822.2004.00397.x

Woodland, J. G., Hunter, R., Smith, P. J., and Egan, T. J. (2017). Shining new light on ancient drugs: preparation and subcellular localisation of novel fluorescent analogues of cinchona alkaloids in intraerythrocytic Plasmodium falciparum. *Org. Biomol. Chem.* 15, 589–597. doi:10.1039/c6ob02110g

Wu, Y. W., Alexandrov, K., and Brunsveld, L. (2007). Synthesis of a fluorescent analogue of geranylgeranyl pyrophosphate and its use in a high-throughput fluorometric assay for rab geranylgeranyltransferase. *Nat. Protoc.* 2, 2704–2711. doi:10.1038/nprot.2007.401

Yoshioka, K., Takahashi, H., Homma, T., Saito, M., Oh, K.-B., Nemoto, Y., et al. (1996). A novel fluorescent derivative of glucose applicable to the assessment of glucose uptake activity of *Escherichia coli*. *Biochim. Biophys. Acta* 1289, 5–9. doi:10.1016/0304-4165(95)00153-0

Zelada, C., Montemartini, M., Cazzulo, J. J., and Nowicki, C. (1996). Purification and partial structural and kinetic characterization of an alanine aminotransferase from epimastigotes of Trypanosoma cruzi. *Mol. Biochem. Parasitol.* 79, 225–228. doi:10.1016/0166-6851(96)02652-7

Zeledon, R. (1960). Comparative physiological studies on four species of hemoflagellates in culture. II. Effect of carbohydrates and related substances and some amino compounds on the respiration. *J. Parasitol.* 46, 541–551. doi:10.2307/3274935

Zingales, B. (2018). Trypanosoma cruzi genetic diversity: something new for something known about chagas disease manifestations, serodiagnosis and drug sensitivity. *Acta Trop.* 184, 38–52. doi:10.1016/j.actatropica.2017.09.017

Zingales, B., Andrade, S. G., Briones, M. R. S., Campbell, D. A., Chiari, E., Fernandes, O., et al. (2009). A new consensus for Trypanosoma cruzi intraspecific nomenclature: second revision meeting recommends TcI to TcVI. *Mem. Inst. Oswaldo Cruz* 104, 1051–1054. doi:10.1590/S0074-02762009000700021

Zingales, B., Miles, M. A., Campbell, D. A., Tibayrenc, M., Macedo, A. M., Teixeira, M. M. G., et al. (2012). The revised Trypanosoma cruzi subspecific nomenclature: rationale, epidemiological relevance and research applications. *Infect. Genet. Evol.* 12, 240–253. doi:10.1016/j.meegid.2011.12.009